7 Dynamics of Solvent and Spectral Relaxation

In the preceding chapter we described the effects of solvent and local environment on emission spectra, and how spectral changes could be used to determine the properties of the environment surrounding a fluorophore. We showed that emission spectra could be affected by solvent polarity and specific solvent effects. We also showed that fluorophores could display charge separation and/or conformational changes while in the excited state. During these descriptions we did not consider the rate constants for these processes, but mostly assumed the lifetime of a fluorophore was in equilibrium with its environment prior to emission. More specifically, we assumed the decay rates of the fluorophores were slow compared to the rate constants for solvent reorientation, charge separation, or conformational changes in the fluorophore. The assumption of emission from equilibrated states was reasonable because fluid solvents reorient around excited fluorophores in 0.1 to 10 ps, and the decay times are typically 1 ns or longer.

There are many situations where the fluorophore can emit prior to or during other dynamic processes. For example, in viscous solvents the rate of solvent relaxation around the fluorophore may be comparable to or slower than the decay rate. In this case the emission occurs during solvent relaxation, and the emission spectrum represents an average of the partially relaxed emission. Under these conditions the emission spectra display time-dependent changes. These time-dependent effects are not observed in the steady-state emission spectra, but can be seen in the time-resolved data or the intensity decays measured at various emission wavelengths. Many fluorophores undergo reactions in the excited state, such as the loss or gain of a proton. Depending on the chemical properties of the fluorophore, its exposure to the solvent, and/or the concentration of proton donors or acceptors in the solution, the excited-state reaction may be occurring during emission. In this case the steady-state spectrum will contain contributions from each form of the fluorophore, assuming that both forms are fluorescent.

As was true for solvent effects, there is no universal theory that provides a quantitative description of all the observed phenomena. Time-dependent shifts occur as the result of general solvent effects, specific solvent-fluorophore interactions, formation of internal charge-transfer states, and excited-state reactions. All of these processes affect the time-dependent decays. Interpretation of the time-resolved data should be based on a molecular understanding of the fluorophore and the nature of its environment. In some cases the effects are often similar and not immediately assignable to a particular molecular event. Hence, it can be challenging to select a model for interpretation of the time-dependent spectra.

7.1. OVERVIEW OF EXCITED-STATE PROCESSES

Prior to consideration of specific mechanisms, it is useful to understand how emission spectra are affected by processes occurring during the excited-state lifetime. We can divide the time-dependent spectral changes into two categories: a continuous spectral shift or a two-state model. In the continuous model the emission spectrum shifts with time but does not change the spectral shape.[1–3] The continuous model is usually appropriate for general solvent effects. In the two-state model there are distinct emission spectral from two forms of the fluorophore. The two-state model is usually appropriate for excited-state reactions or formation of internal charge-transfer (ICT) states.

Excited-state processes are usually studied by measurement of the time-resolved emission spectra (TRES). The TRES are the emission spectra that would be observed if measured at some instant in time following pulsed excitation. Figure 7.1 shows a schematic for the continuous spectral relaxation (CR) model. The fluorophore is excited to the Franck-Condon (F) or unrelaxed state. Following excitation the solvent reorients around the excited-state dipole moment, which occurs with a solvent relaxation rate k_s,

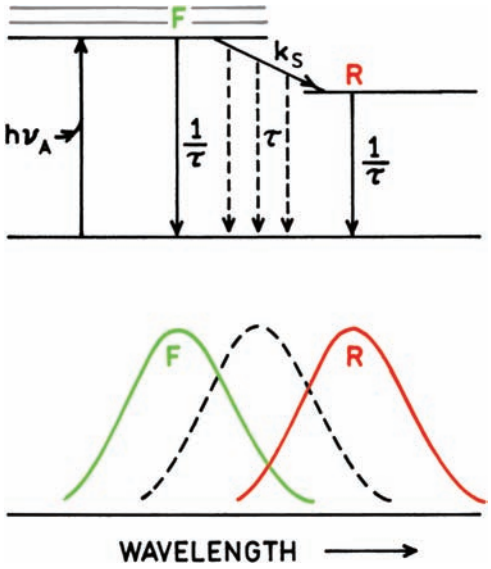

Figure 7.1. Jablonski diagram for continuous spectral relaxation.

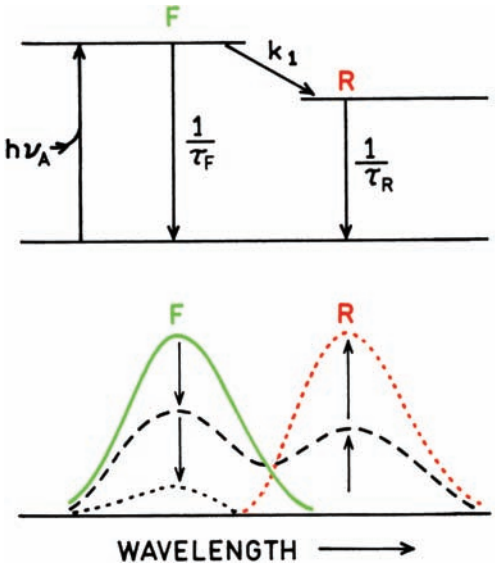

Figure 7.2. Jablonski diagram for an excited-state reaction.

which can also be described by a solvent relaxation time $\tau_s = k_s^{-1}$. If the solvent is fluid the solvent relaxation time will be less than the lifetime ($\tau_s << \tau$) and emission occurs from the relaxed (R) state. At low temperature, solvent relaxation can be slower than emission ($\tau_s >> \tau$) so that emission is observed from the F state. At intermediate temperature emission where $\tau_s = \tau$ emission will be occurring during the relaxation process. Hence a spectrum intermediate between F and R will be observed (dashed curve in Figure 7.1), which represents some weighted average of the emission spectra at each point in time during the relaxation process. In rigorous terms the intermediate spectrum would have the same shape and half width as the F- and R-state emission spectra. In practice the intermediate spectrum can be wider due to contributions from fluorophores with varying extents of relaxation. In Figure 7.1 we show the same lifetime τ for the fluorophore in the F and R state because the fluorophore is emitting from the same electronic state. In practice these decay times can be different.

Spectral relaxation can also occur in a stepwise manner, which we will call the excited-state reaction (ESR) model. In this case there are two distinct emitting species: the initially excited state F and the species R resulting from the excited-state reaction. The lifetime of the F and R states (τ_F and τ_R) are different because emission is occurring from a different molecular species (Figure 7.2). In the case of excited-state ionization the emission would be from the initially excited and the ionized species. The F and R states can also have different emission spectra because the electronic states or chemical structures are different.

For the ESR model the F and R states are linked by a rate constant k_1. The reaction can be reversible, but for simplicity is shown as an irreversible reaction. The rate constant k_1 is now a chemical rate constant that is determined by the chemical structures and solvent composition. If the rate constant is small relative to the decay rate of the F state ($k_1 < \tau_F^{-1}$) the emission occurs mostly from the F state. If the reaction rate is greater than the decay rate of the F state ($k_1 > \tau_F^{-1}$) then emission occurs primarily from the R state. If the reaction rate and decay rates are comparable then emission occurs from both species. If the emission spectra of the F and R states are well separated then two distinct components will be seen in the emission spectrum. If the emission spectra of the F and R states overlap, the intermediate emission spectra may show a shoulder or be wider than the individual emission spectra.

The continuous relaxation and ESR models can also be described in terms of reaction coordinates. In the CR model emission is occurring from the same state (Figure 7.3), except for a displacement due to solvent reorientation. The rate constant k_s describes the rate at which the excited-state energy slides towards the equilibrium R state. Emission occurs at all positions along the reaction coordinate. For the ESR model there are two excited-state species, typically separated by an energy barrier (Figure 7.4). Emission can occur from either state, but the states are distinct. The rate

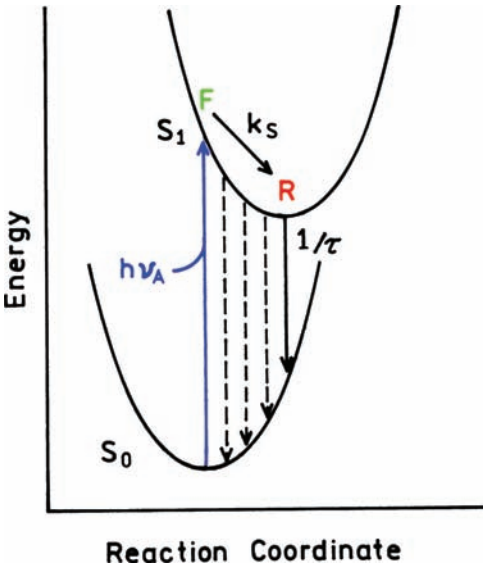

Figure 7.3. Energy schematic for continuous spectral relaxation.

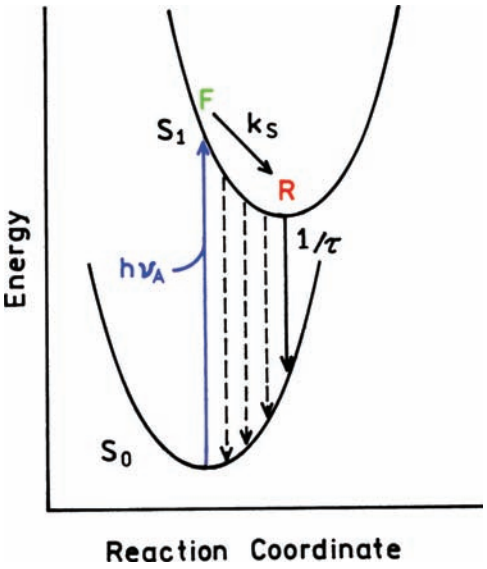

Figure 7.4. Energy schematic for an excited-state reaction.

constant k_1 describes the rate at which the F state is transformed into the R state.

7.1.1. Time-Resolved Emission Spectra

Excited-state processes result in complex time-dependent decays. The intensity decays depend on the observation wavelength because of the time needed for the F state to become an R state or some intermediate state. This situation is illustrated in Figure 7.5. In this figure the solid line shows the intensity decay of the total emission, or the decay that would be observed in the absence of excited-state processes. Now suppose the intensity decay is measured on the short-wavelength side of the total emission. This decay, $I_F(t)$, is more rapid than the decay of the total emission, $I_T(t)$, because the short-wavelength emission is decaying by both emission and relaxation, which is removing excited fluorophores from the observation wavelength. On the long-wavelength side of the emission the emitting fluorophores are those that have relaxed.

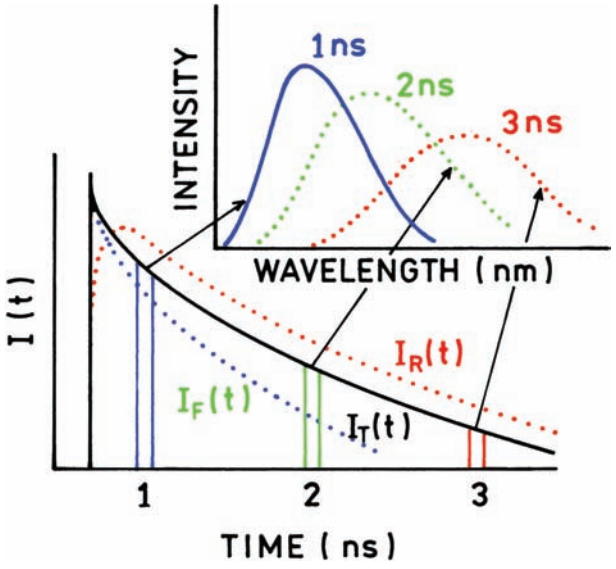

Figure 7.5. Schematic of time-resolved emission spectra. $I_T(t)$ represents the decay of the total emission. $I_F(t)$ and $I_R(t)$ are the intensity decays on blue and red sides of the emission spectrum, respectively. The upper insert shows the emission spectra at t = 1, 2, or 3 ns.

Time is needed for the F-state molecules to reach the R state. Even if the F and R states have the same intrinsic decay time, the long-wavelength decay will appear to be slower. Also, at the moment of excitation all the molecules are assumed to be in the F state. No molecules are in the R state until some relaxation has occurred. For this reason one typically observes a rise in the intensity at long wavelengths representing formation of the relaxed state. The rise time is frequently associated with a negative pre-exponential factor that is recovered from the multi-exponential analysis. Following the rise in intensity, the decay $I_R(t)$ typically follows the total emission. Another way of understanding the wavelength-dependent decays is to recall that emission is a random event. Some fluorophores emit at earlier times, and

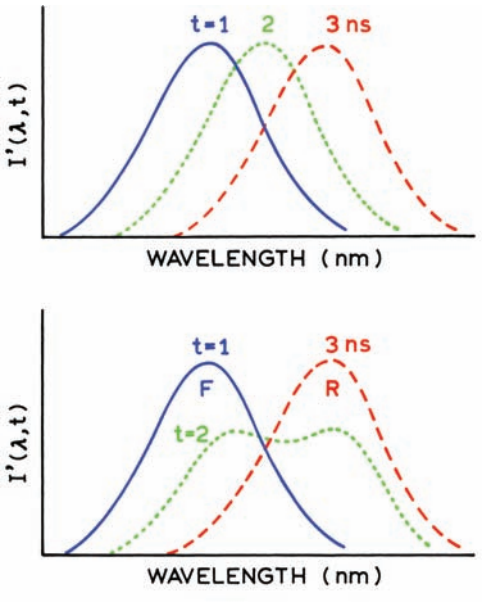

Figure 7.6. Normalized time-resolved emission spectra for continuous relaxation (top) and for a two-state process (bottom).

some at later times. The decay rate represents the ensemble average. The fluorophores that emit at earlier times tend to have shorter wavelength emission, and those that emit at later times have longer wavelength emission.

Suppose that emission spectra could be recorded at any desired instant following the excitation pulse (Figure 7.6) and that the spectra are normalized. First consider a continuous relaxation process (top panel). If the emission spectrum was observed immediately after excitation (t = 1 ns), then a blue-shifted or unrelaxed emission will be observed. If the time of observation is later, then more of the molecules will have relaxed to longer wavelengths, resulting in emission spectra that are progressively shifts to longer wavelengths at longer times. For continuous spectral relaxation the shape of the emission spectra are expected to remain the same. Now consider the ESR model (Figure 7.6, lower panel). At short times the blue-shifted emission would be observed. At long times the emission would be from the reacted fluorophore. At intermediate times emission from both species would be observed. Typically the emission spectrum would be wider at intermediate times due to emission from both forms of the fluorophore. These emission spectra, representing discrete times following excitation, are called the time-resolved emission spectra (TRES). It is technically challenging to determine the TRES, and the molecular interpretation can be equally difficult.

7.2. MEASUREMENT OF TIME-RESOLVED EMISSION SPECTRA (TRES)

7.2.1. Direct Recording of TRES

The measurement of TRES is most easily understood using pulse sampling or time-gated detection (Chapter 4). In fact, the first reported TRES were obtained using this method,[4–6] but this method is rarely used at the present time. The sample was 4-aminophthalimide (4-AP) in propanol at –70°C. At this temperature the rate of solvent relaxation is comparable to the decay time. The sample is excited with a brief pulse of light, and the detector was gated on for a brief period (typically <0.5 ns) at various times following the excitation pulse. The emission spectrum is then scanned as usual. For short time delays a blue-shifted emission was observed (Figure 7.7). As the delay time was increased, the emission spectrum shifted to longer wavelength. At these longer times the solvent has relaxed around the excited-state dipole.

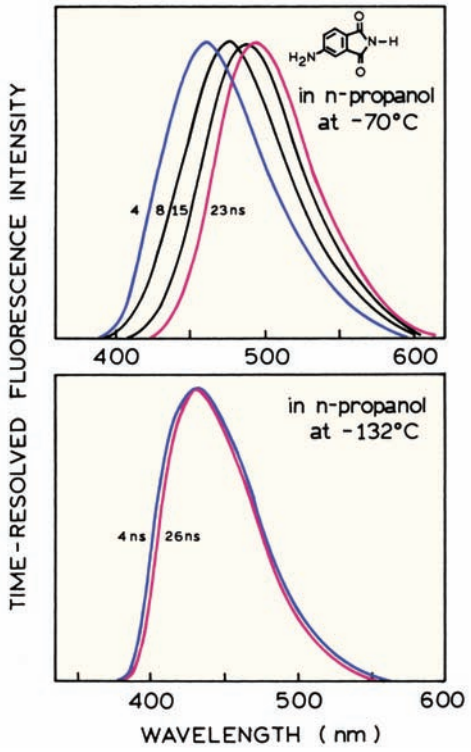

Figure 7.7. Time-resolved fluorescence spectra of 4-aminophthalimide in n-propanol at –70 and –132°C recording using the pulse sampling method (Chapter 4). The times between excitation and gated sampling of the emission intensity are listed on the figures. Revised from [4].

Examination of Figure 7.7 reveals that the shape and/or width of the emission spectrum is not changed during spectral relaxation. This suggests that relaxation of 4-aminophthalimide in n-propanol proceeds as a continuous process. When the temperature was lowered to –132°C the emission spectra were similar for time delays of 4 and 26 ns. This is because at lower temperatures the relaxation time of the solvent is longer than the decay time of 4-aminophthalimide, which is near 10 ns.

TRES have also been obtained using TCSPC. When using TCSPC one can record photons arriving within a small time interval. In this instance one selects the output pulses from the TAC to be within a limited range of voltage values. The range of accepted voltages determines the time window that is observed. The emission spectrum is then recorded with a monochromator. While intuitively simple, this method is rather inefficient and has not been widely utilized.

Direct recording of TRES is easy to understand, but this procedure has a serious limitation. The directly recorded TRES do not provide for deconvolution using the instrument response function. Hence the recorded TRES are apparent spectra containing distortions due to the instrument response function. One exception is use of the pump-probe or upconversion methods, when the time resolution can be fast compared to the rates of spectral relaxation.

7.2.2. TRES from Wavelength-Dependent Decays

At present, time-resolved emission spectra are usually obtained indirectly. The procedure starts with measurement of the time-resolved decays at a number of wavelengths across the emission spectrum, $I(\lambda,t)$.[7–9] The intensity decays are wavelength dependent. The short wavelengths decay more rapidly than the longer wavelengths. This occurs because the emission on the short-wavelength side of the spectrum is decaying by both emission and by relaxation to longer wavelengths. In contrast, the emission at long wavelengths requires that the fluorophores relax prior to emission, and is thus delayed by the relaxation time.

For calculation of the TRES the intensity decays are usually analyzed in terms of the multi-exponential model

$$I(\lambda,t) = \sum_{i=1}^{n} \alpha_i(\lambda) \exp\left[-t/\tau_i(\lambda)\right] \qquad (7.1)$$

where $I(\lambda,t)$ are the intensity decays at each wavelength, $\alpha_i(\lambda)$ are the pre-exponential factors, $\tau_i(\lambda)$ are the decay times, with $\Sigma\alpha_i(\lambda) = 1.0$. In this analysis the decay times can be variables at each wavelength $\tau_i(\lambda)$, or assumed to be independent of wavelength, τ_i. Wavelength-dependent decay times are expected for the continuous model, and wavelength-independent lifetimes are expected for the two-state model. However, because of limited resolution and parameter correlation, the data can usually be fit with either wavelength-dependent $\tau_i(\lambda)$ or wavelength-independent τ_i lifetimes, irrespective of whether relaxation is a continuous or two-state process. For purposes of calculating the TRES the choice does not matter as long as good fits are obtained. The goal is to obtain a parametrized form of the intensity decays, which are then used to reconstruct the TRES. Typically, no molecular significance is assigned to the intensity decay parameters.

In order to calculate the TRES one computes a new set of intensity decays, which are normalized so that the time-integrated intensity at each wavelength is equal to the steady-state intensity at that wavelength. Suppose $F(\lambda)$ is the steady-state emission spectrum. One calculates a set of $H(\lambda)$ values using

$$H(\lambda) = \frac{F(\lambda)}{\int_0^\infty I(\lambda,t)\,dt} \qquad (7.2)$$

which for the multi-exponential analysis becomes

$$H(\lambda) = \frac{F(\lambda)}{\sum_i \alpha_i(\lambda)\tau_i(\lambda)} \qquad (7.3)$$

These equations can be understood as follows. The term $H(\lambda)$ is the volume that, when multiplied by the time-integrated intensity at the same wavelength, is equal to the steady-state intensity at that wavelength. Then, the appropriately normalized intensity decay functions, which are used to calculate the TRES, are given by

$$I'(\lambda,t) = H(\lambda)I(\lambda,t) = \sum_i \alpha'_i(\lambda) \exp\left[-t/\tau_i(\lambda)\right] \qquad (7.4)$$

where $\alpha_i'(\lambda) = H(\lambda)\alpha_i(\lambda)$.

The values of $I'(\lambda,t)$ can be used to calculate the intensity at any wavelength and time, and thus the TRES. The TRES can be shown with the actual intensities, as in Figure 7.5, or peak normalized, as shown in Figures 7.6 (top) and 7.7 (lower panel). Assuming the intensity decays have been measured at an adequate number of wavelengths, this procedure (eqs. 7.1–7.4) yields the actual TRES independent of

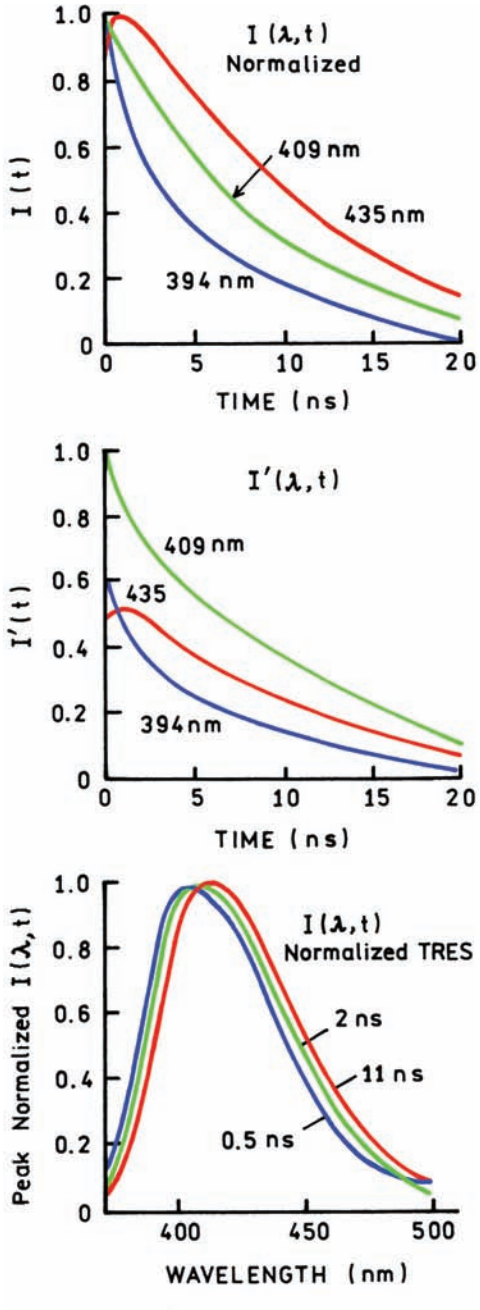

Figure 7.8. Calculation of time-resolved emission spectra. Revised from [9].

the nature of the relaxation process. The advantage of this procedure is that the values of I'(λ,t) are the actual impulse response functions, corrected for distortions due to convolution with the instrument response function. The time dependence of the spectral shifts, and the shape of the TRES, are then used to determine the rates of relaxation and the nature of the relaxation process.

The calculation of TRES from the measured intensity decays is best understood by a specific example (Figure 7.8). This example is for the probe 2-anilinonaphthalene (2-AN) bound to phospholipid vesicles,[9–10] but the procedure is the same for any sample. The time-resolved decays are measured at appropriate wavelengths across the entire emission spectrum. Typical decays at 394, 409, and 435 nm are shown in the upper panel. The time-resolved decays are used to derive the impulse response functions at each emission wavelength, $I(\lambda,t)$. These decays were obtained using an unusual deconvolution calculation (Figure 7.8, top panel). A multi-exponential fit is used, but no physical significance is attached to the values of $\alpha_i(\lambda)$ and $\tau_i(\lambda)$. These are simply used to obtain an accurate representation for the observed intensity decays. One may interpret these results as follows. At shorter wavelengths the intensity decay is faster due to spectral relaxation. At longer wavelengths one selectively observes those fluorophores that have relaxed, and hence those that have emitted at later times following excitation. Thus the overall decay is slower at longer wavelengths.

The decays at each wavelength are then normalized so the time-integrated areas for each wavelength are equal to the steady-state intensity at that wavelength (middle panel). These decays are then used to calculate the emission spectra for any desired time following the excitation pulse. The TRES are usually peak normalized to allow easy visualization of the time-dependent spectral shifts. For 2-AN bound to vesicles one notices that the spectra shift to longer wavelengths at longer times (bottom panel).

Examination of Figure 7.8 (top and middle panels) shows a characteristic feature of solvent relaxation, which is a rise in intensity at long wavelengths (435 nm). This rise occurs because at $t = 0$ no fluorophores are in the relaxed state. The population of the relaxed state increases prior to decreasing due to the total intensity decay. Observation of such a term provides proof that an excited-state process has occurred. If the sample displayed only ground-state heterogeneity, then the decays would be dependent upon wavelength. However, no rise in intensity would be observed for ground state heterogeneity because all the pre-exponential factors would be positive (Section 7.11).

7.3. SPECTRAL RELAXATION IN PROTEINS

Time-resolved emission spectra have been used to study the dynamics of proteins and membranes. The basic idea is that excitation provides an instantaneous perturbation because

of the increased dipole moment of the excited state. If the biomolecule is rigid, there will be no relaxation, as was seen for 4-AP in propanol at –132°C (Figure 7.7). If the biomolecule is flexible, then the TRES should relax on a timescale characteristic of the macromolecule. Time-dependent spectral shifts have been observed for probes bound to proteins,[11–21] membranes,[22–33] micelles,[34–39] and polymers,[40–41] and has recently been reviewed.[42] Spectral relaxation of intrinsic tryptophan fluorescence in proteins will be described in Chapter 17.

7.3.1. Spectral Relaxation of Labeled Apomyoglobin

One example of TRES of a protein is provided by labeled myoglobin. Myoglobin is a muscle protein that binds oxygen from the blood and releases oxygen as needed to the muscles. Myoglobin thus acts as an oxygen reservoir. In myoglobin the oxygen molecule is bound to the heme group, which is near the center of the protein. The heme group can be removed from the protein, leaving a hydrophobic pocket that is known to bind a number of fluorophores.[43–44] Myoglobin without the heme group is called apomyoglobin. The dynamics of myoglobin are of interest because myoglobin cannot bind and release oxygen without undergoing structural fluctuations to allow diffusion of oxygen through the protein. If the protein is flexible on the nanosecond timescale for oxygen penetration, then it seems likely the protein can be flexible during the nanosecond decay times of bound fluorophores.

In the previous chapter we described Prodan and its derivatives as being highly sensitive to solvent polarity. The dynamics of the heme binding site was studied using the probe Danca, which is an analogue of Prodan (Figure 7.9). The carboxy cyclohexyl side chain serves to increase the affinity of Danca for apomyoglobin, and to ensure it binds to the protein in a single orientation. A single mode of binding simplifies interpretation of the data by providing a homogeneous probe population. Excitation of Danca results in the instantaneous creation of a new dipole within the apomyoglobin molecule. If myoglobin is flexible on the ns timescale, one expects time-dependent shifts in its emission spectrum as the protein rearranges around the new dipole moment.

Intensity decays were measured at various wavelengths across the emission spectrum (Figure 7.9). The amplitudes of these decays were adjusted according to eq. 7.3. The decays are somewhat faster at shorter emission wavelengths. Importantly, there is evidence of a rise time at longer wavelengths, which is characteristic of an excited-state process. A rise time can only be observed if the emission is not directly excited, but rather forms from a previously excited state. In this case the initially excited state does not contribute at 496 and 528 nm, so that the decays at these wavelengths show an initial rise in intensity. The emission at these wavelengths is due to relaxation of the initially excited state.

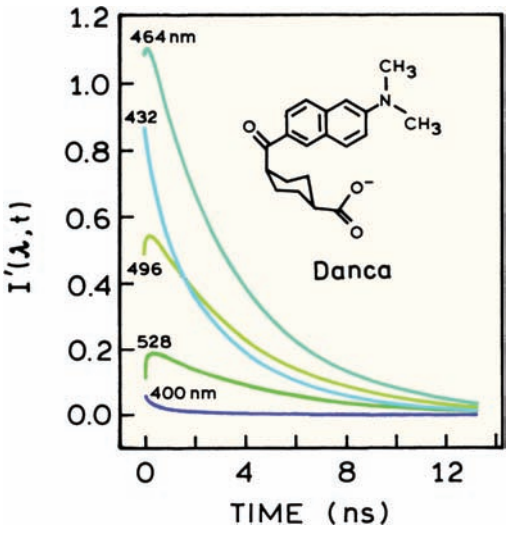

Figure 7.9. Deconvolved fluorescence decays of Danca-apomyoglobin complex from 400 to 528 nm at 298°K. The area under each trace has been scaled to the steady-state intensity at that wavelength. Note the intensity decays show a rise time at longer wavelengths. Revised and reprinted with permission from [17]. Copyright © 1992, American Chemical Society.

The time-dependent decays were used to construct the time-resolved emission spectra (Figure 7.10). These spectra shift progressively to longer wavelength at longer times. Even at the earliest times (20 ps) the TRES are well shifted from the steady-state spectrum observed at 77°K. At this low temperature solvent relaxation does not occur. As was described in Chapter 6 (Figure 6.28), Prodan-like molecules can emit from locally excited (LE) and internal charge-transfer (ICT) states. The short-wavelength emission at 77°K is probably due to the LE state. Hence, the emission of DANCA-apomyoglobin is from the ICT state, which has undergone nearly complete charge separation.

The TRES can be used to calculate the rates of spectral relaxation. These data are usually presented as the average energy of the emission versus time (Figure 7.11). Alternatively, one can calculate the time-dependent change in the emission maximum. In the case of Danca-apomyoglobin

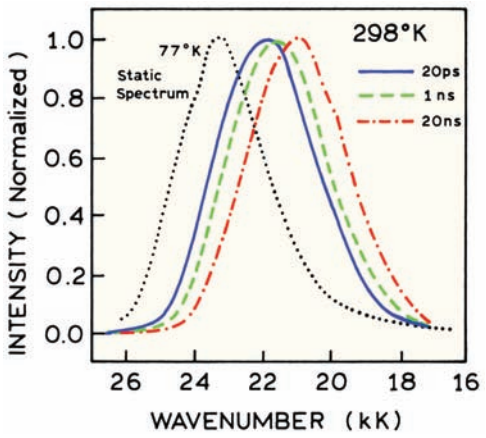

Figure 7.10. Time-resolved emission spectra of Danca bound to apomyoglobin. Also shown is the steady-state spectrum at 77°K. Revised and reprinted with permission from [17]. Copyright © 1992, American Chemical Society.

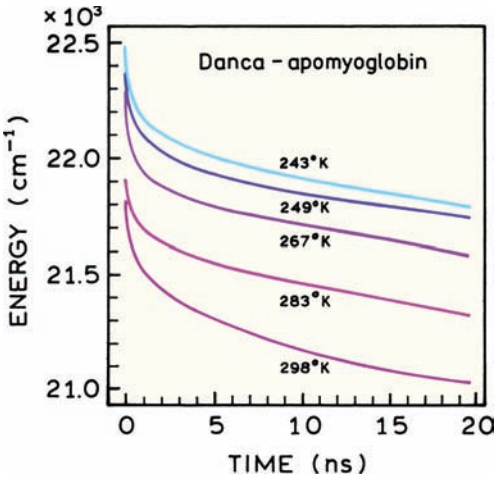

Figure 7.11. Decay of the mean energy of the emission (in cm^{-1}) of Danca-apomyoglobin at various temperatures in water and glycerol-water mixtures. Revised and reprinted with permission from [17]. Copyright © 1992, American Chemical Society.

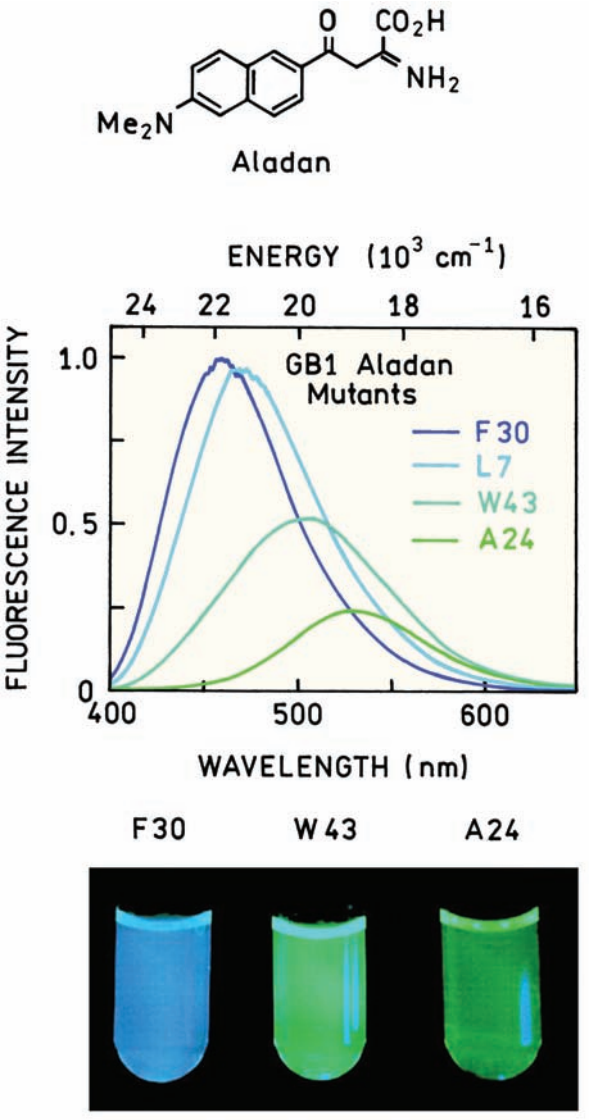

Figure 7.12. Emission spectra and color photographs of GB1 mutants containing Aladan in the sequence. Revised from [45].

the decay of the average energy was highly non-exponential, and with relaxation times ranging from 20 ps to 20 ns. Spectral relaxation is typically a multi- or non-exponential process for probes in solvents or when bound to macromolecules. Methods used to determine the relaxation times are described below.

7.3.2. Protein Spectral Relaxation Around a Synthetic Fluorescent Amino Acid

The previous example showed relaxation of apomyoglobolin around a Prodan analogue, which occurred in about 10 ns. It was not clear if a-10 ns relaxation time was typical of proteins or a consequence of the artificial probe in the heme binding site. Hence it was of interest to measure spectral relaxation in an unperturbed protein. Tryptophan is one choice as a probe, but it is usually more difficult to perform high time-resolution experiments with UV excitation and emission wavelengths. To minimize the effects of labeling a synthetic amino acid was synthesized that was analogous to Prodan (Aladan in Figure 7.12).[46] This amino-acid analogue was incorporated into the B1 domain of streptococcal protein G (GB1). This protein binds to IgG and is frequently used as a model for protein

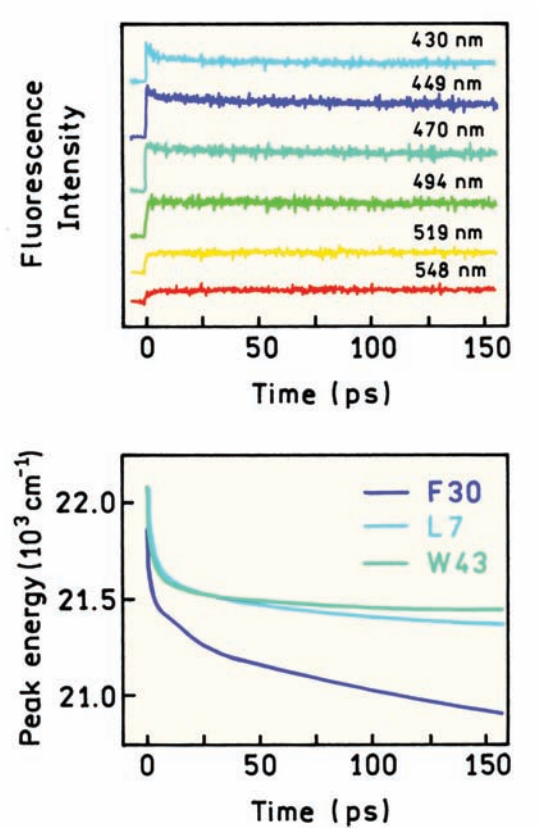

Figure 7.13. Time-dependent intensity decays and time-dependent peak emission energy of the F30 Aladan mutant of GB1 measured using fluorescence upconversion. The lower panel shows the time-dependent peak energy for three mutants of GB1. Revised from [45].

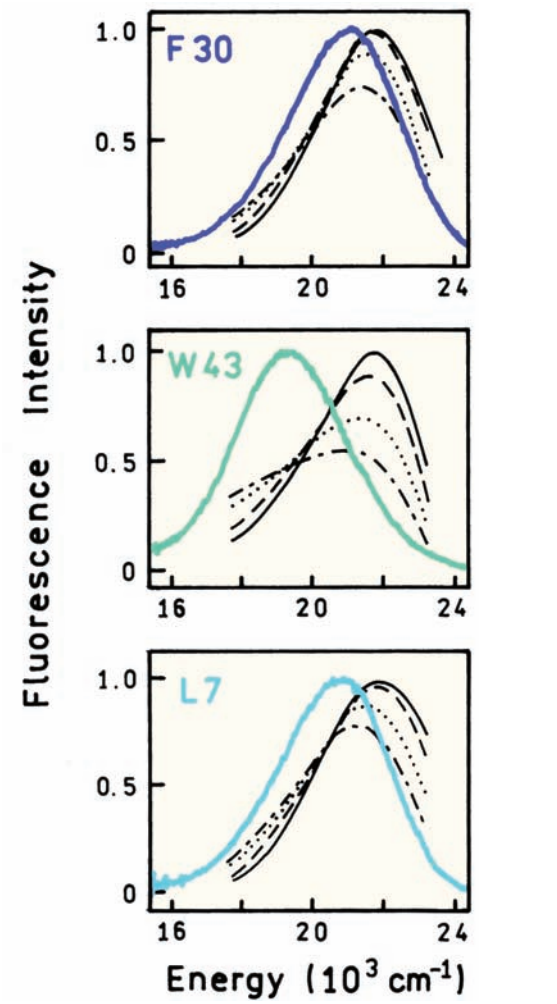

Figure 7.14. Time-resolved and steady-state emission spectra for GB1 mutants with Aladan in the sequence. The thick lines are the steady-state emission spectra. The time-resolved spectra are at 200 fs (solid lines), 1 ps (dashed line), 10 ps (dotted lines) and 150 ps (dot dashed lines). Revised from [45].

folding.[47] Figure 7.12 shows the emission spectra of Aladan-GB1 when Aladan is incorporated into four different sites. The emission maxima are different for each mutant, showing that the Aladan residue can be shielded, partially exposed, or exposed to the aqueous phase.

Time-dependent decays are needed to calculate the TRES (Figure 7.13). For Aladan-GB1 the wavelength-dependent parts of the decays were complete in about 20 ps, much faster than for Danca-labeled apomyoglobin. The 20-ps timescale is too fast for reliable TCSPC measurements, so these decays were recorded using fluorescence upconversion. The intensity decays were used to calculate the TRES (Figure 7.14). The time-dependent shifts were found to occur over a range of timescales. There is a rapid component that occurs in less than 20 ps (Figure 7.13, lower panel) and a slower shift occurring over several nanoseconds. Presumably, these slower components will result in the emission spectra becoming similar to the steady-state spectra (thick lines in Figure 7.14).

7.4. SPECTRAL RELAXATION IN MEMBRANES

Time-resolved emission spectra have been extensively used to study membrane dynamics.[24–33] While not intuitively obvious, frequency-domain data can also be used to determine TRES, as will be shown for Patman-labeled DPPC vesicles. Patman is also a Prodan derivative, in this case designed to bind to membranes (Chapter 6, Figure 6.20). As for the time-domain measurements, the frequency-domain data are measured for various wavelengths across the emission spectrum (Figure 7.15). The phase and modulation values are strongly dependent on emission wavelength. At 46°C on the blue side of the emission, the phase angles are

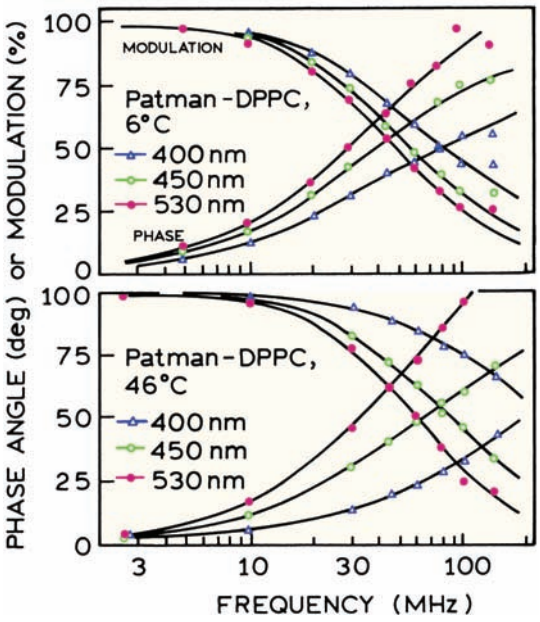

Figure 7.15. Frequency-dependent phase and modulation values for Patman-labeled DPPC vesicles. Top, 6°C; bottom, 46°C. For both temperatures, data are shown for 400 (Δ, 450 (○) and 530 nm (●). Revised from [26]. Copyright © 1984, with permission from Elsevier Science.

Table 7.1. Intensity Decays of Patman-Labeled DPPC Vesicles[a]

Wavelength	6°C (τ, ns) (0.98 ns) α_1 (λ)[b]	(3.74 ns) α_2 (λ)	(5.52 ns) α_3 (λ)
400	1.15	0.60	0.25
430	0.21	1.02	0.77
450	–0.13	0.95	0.92
470	–0.40	0.73	0.87
490	–0.50	0.57	0.93
510	–0.61	0.33	1.06
530	–0.74	0.18	1.08
Wavelength	46°C (τ, ns) (0.95 ns) α_1 (λ)	(1.48 ns) α_2 (λ)	(3.94 ns) α_3 (λ)
400	1.84	–	0.16
430	0.52	1.16	0.32
450	–0.56	0.91	0.53
470	–0.77	0.45	0.78
490	–0.85	0.14	1.01
510	–0.71	–0.20	1.09
530	–0.50	–0.42	1.08

[a]From [26].
[b]The sum of the absolute values of $\alpha_i(\lambda)$ are set to 2.0 at each wavelength.

shorter and the modulation values higher than on the red side of the emission. The phase angles on the red side of the emission exceed 90°, which is proof of an excited-state reaction. The data at low temperature (6°C) are also characteristic of an excited-state process, larger phase angles, and lower modulation on the long-wavelength side of the emission. However, the long-wavelength phase angles are less obviously in excess of 90°. An absence of phase angles over 90° does not prove relaxation has not occurred, only that the conditions were not suited to result in very large phase angles.

The phase and modulation data can be used to derive the wavelength-dependent impulse response functions. In this case the data at all wavelengths could be fit to a set of three wavelength-independent lifetimes (Table 7.1). The three decay times are similar at both 8 and 46°C. The main distinction between the high- and low-temperature data is the larger contribution of terms with negative pre-exponential factors at the higher temperature. Phase angles in excess of 90° in the frequency-domain data are similar to negative pre-exponential factors in the time-domain. At the longest emission wavelength these positive and negative terms are nearly equal in magnitude and opposite in sign. This is characteristic of emission from a relaxed state that can be observed without a substantial contribution from the initially excited state.[48]

The recovered impulse response functions (Table 7.1) can be used to calculate the time-resolved emission spectra (Figure 7.16). To facilitate comparison of these spectra we chose to display normalized time-resolved spectra at 0.2, 2, and 20 ns. For DPPC, below its transition temperature near 37° there is only a modest red shift of 15 nm at 20 ns. At 46°C a dramatic spectral shift is seen to occur between 0.2 and 20 ns, about 50 nm. These TRES indicate that the extent and/or rate of spectral relaxation are greater at the higher temperature. At 2 ns and 46°C, the time-resolved emission spectrum of Patman appears wider than at 0.2 or 20 ns. This suggests a two-state model for spectra relaxation. Specifically, at 46°C and 2 ns emission is observed from both the unrelaxed and relaxed states of Patman.

7.4.1. Analysis of Time-Resolved Emission Spectra

The time-dependent spectral shifts can be characterized by the time-dependent center of gravity, in wavenumbers (cm^{-1} or kK). The center of gravity is proportional to the average energy of the emission. The center of gravity of the emission is defined by

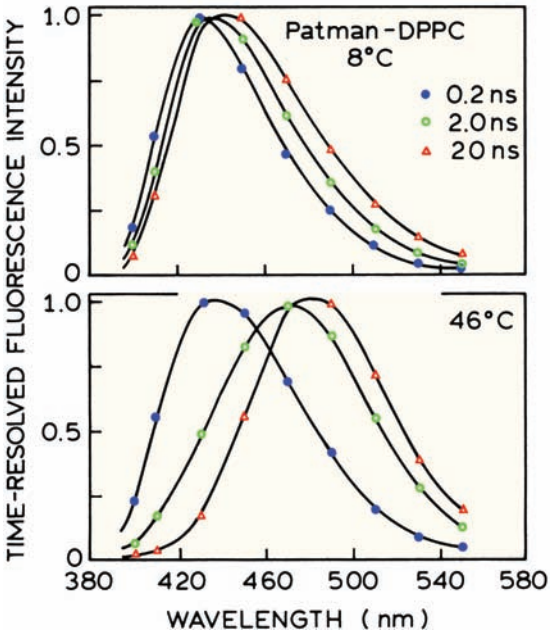

Figure 7.16. Time-resolved emission spectra of Patman-labeled DPPC vesicles. Top, 8°C; bottom, 46°C. Time-resolved spectra are shown at 0.2 (●), 2 ($○$) and 20 ns (D). Revised from [26]. Copyright © 1984, with permission from Elsevier Science.

$$\bar{\nu}_{cg}(t) = \frac{\int_0^\infty I'(\bar{\nu},t)\ \bar{\nu}\, d\bar{\nu}}{\int_0^\infty I'(\bar{\nu},t)\, d\bar{\nu}} \tag{7.5}$$

where $I'(\bar{\nu},t)$ represents the number of photons per wavenumber interval. These are the intensity decays as normalized in eq. 7.4, but on the wavenumber scale. The data are typically collected for selected wavelengths, and the center of gravity in kK (= 10^3 cm^{-1}) is calculated using

$$\bar{\nu}_{cg}(t) = 10{,}000\, \frac{\Sigma_\lambda I'(\lambda,t)\ \lambda^{-1}}{\Sigma_\lambda I'(\lambda,t)} \tag{7.6}$$

Note that the integral in eq. 7.5 is over the emission spectrum ($\bar{\nu}$), and not over time. The TRES at any instant in time are used to calculate $\bar{\nu}_{cg}(t)$ at the chosen time. The calculated center of gravity is typically an approximation since the time-resolved data are not collected at all wavelengths. Also, a vigorous calculation of the center of gravity requires use of the corrected emission spectra on the wavenumber scale. Equation 7.6 is simply an expression which uses the available data ($I'(\lambda,t)$) to obtain an approximate value of $\bar{\nu}_{cg}(t)$.

The time-dependent emission centers of gravity are shown in Figure 7.17 (top panel). It is apparent that the extent of relaxation is greater at 46°C than at 8°C. The rate of relaxation is somewhat faster at the higher temperature. If desired, the values of $\bar{\nu}_{cg}(t)$ versus time can be fit to multi-exponential (eq. 7.15, below) or other non-exponential decay laws for $\bar{\nu}_{cg}(t)$.

The time-dependent spectral half width $\Delta\bar{\nu}(t)$ (cm^{-1}) can be used to reveal whether the spectral relaxation is best described by a continuous or two-step model. This half width can be defined in various ways. One method is to use a function comparable to a standard deviation. In this case $\Delta\bar{\nu}(t)$ can be defined as

$$[\Delta\bar{\nu}(t)]^2 = \frac{\int_0^\infty (\bar{\nu} - \bar{\nu}_{cg}(t))^2 I'(\bar{\nu},t)\, d\bar{\nu}}{\int_0^\infty I'(\bar{\nu},t)\, d\bar{\nu}} \tag{7.7}$$

For calculation of $\Delta\bar{\nu}(t)$ one uses the TRES calculated for a chosen time t and integrates eq. 7.7 across the emission spectrum. For data collected at various wavelengths in nanometers the value of $\Delta\bar{\nu}(t)$ in kK is given by

$$[\Delta\bar{\nu}(t)]^2 = \frac{\sum_\lambda [10{,}000/\lambda - \bar{\nu}_{cg}(t)]^2 I'(\lambda,t)}{\sum_\lambda I'(\lambda,t)} \tag{7.8}$$

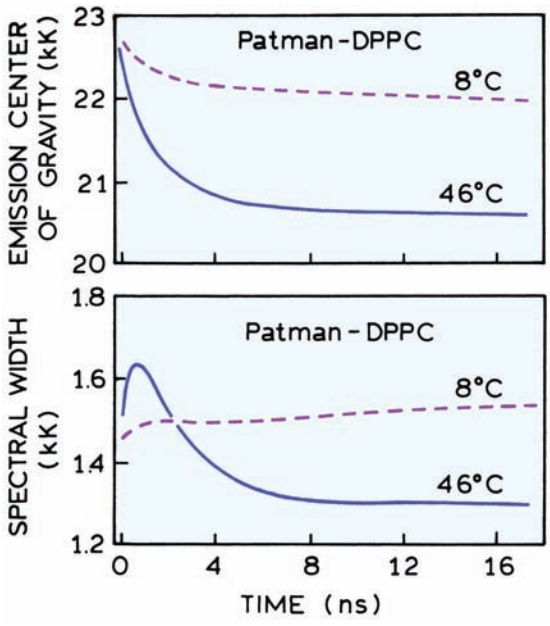

Figure 7.17. Time-resolved emission center of gravity (top) and spectral half width (bottom) of Patman-labeled DPPC vesicles. Revised from [26]. Copyright © 1984, with permission from Elsevier Science.

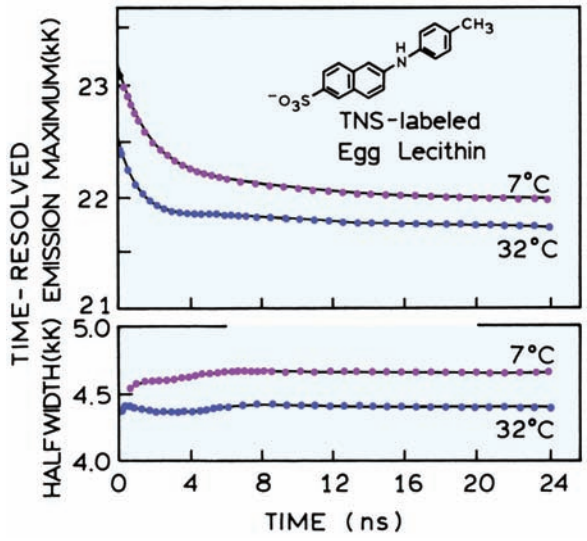

Figure 7.18. Time-resolved emission maxima and spectral half widths for TNS-labeled egg lecithin. Redrawn from [48].

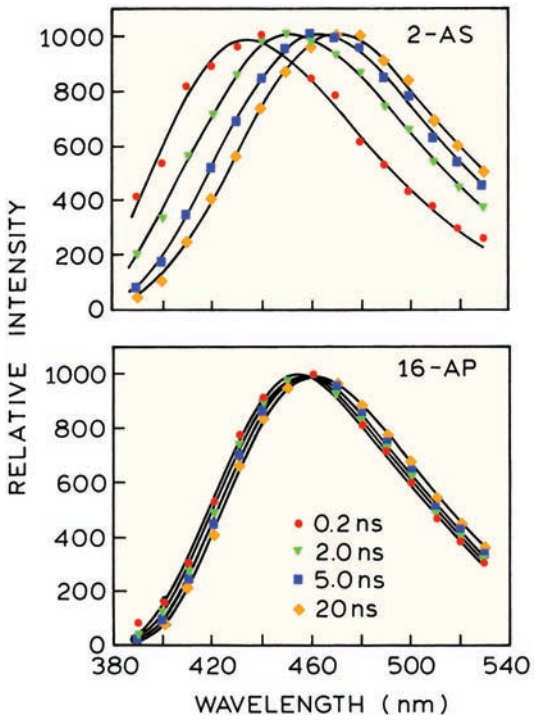

Figure 7.19. Time-resolved emission spectra of anthroyloxy fatty acids (2-AS and 16-AP) in egg phosphatidylcholine vesicles. Revised from [29].

Examination of the time-dependent value of $\Delta\bar{\nu}(t)$ can reveal the nature of the relaxation process. For Patman in DPPC vesicles at 46°C there is an increase in half width at intermediate times. This suggests that spectral relaxation around Patman is best described as a two-state process. Such behavior is not seen for all probes. For TNS-labeled vesicles[26,48] the half-width remains constant during spectral relaxation (Figure 7.18). This suggests that relaxation around TNS is best described by a continuous process in which an emission spectrum of constant shape slides to longer wavelengths.

7.4.2. Spectral Relaxation of Membrane-Bound Anthroyloxy Fatty Acids

Another example of spectral relaxation in membranes is the anthroyloxy fatty acids, which have been extensively used as membrane probes. One advantage of these probes is that the fluorophore can be localized at the desired depth in the membrane by its point of attachment to the fatty acid. The localized anthroyloxy groups have been used to study the dynamics of spectral relaxation at various depths in membranes. The time-resolved emission spectra of these probes are sensitive to the location of the probe in these membranes.[29] This is seen by the larger time-dependent shifts for 2-AS than for 16-AP (Figure 7.19). At first glance this difference seems easy to interpret, with larger spectral shifts for the probe located closer to the polar membrane-water interface. However, closer inspection reveals that the emission spectra of 16-AP are more shifted to the red at early times following excitation. This is evident from the time-dependent emission maxima (Figure 7.20). It seems that the probes located deeper in the bilayer should display a more blue-shifted emission. The reason for the larger red shift of 16-AP is not understood at this time. However, it is thought that the anthroyloxy probes near the ends of acyl chains can fold back to the lipid–water interface. The data in Figure 7.20 are consistent with the fluorophores in both 12-AS and 16-AP being localized near the lipid–water interface.

The rates of spectral relaxation for the anthroyloxy probes also seem to be unusual. The fluidity of lipid bilayers is thought to increase towards the center of the bilayer. Examination of the time-dependent emission maxima (Figure 7.20) suggests that the relaxation becomes slower for probes localized deeper in the membranes. This is seen more clearly in the correlation functions (eq. 7.12, below), which display the relaxation behavior on a normalized scale (Figure 7.21). The apparent relaxation times increase from 2.7 to 5.9 ns as the anthroyloxy moiety is attached more distant from the carboxy group. These results can be understood by the membrane becoming more fluid near the cen-

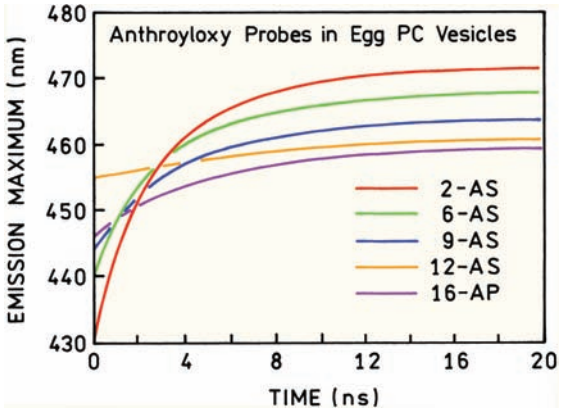

Figure 7.20. Time-dependent emission maxima of anthroyloxy fatty acids in egg PC vesicles. Dots: 2-AS; triangles: 6-AS: boxes: 9-AS; circles: 12-AS; asterisks: 16-AP. Revised from [29].

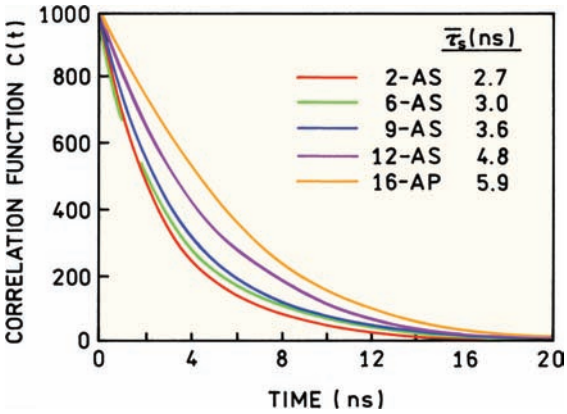

Figure 7.21. Correlation functions for spectral relaxation of the anthroyloxy fatty acids in egg PC vesicles. Revised from [29].

ter, if the 12-AS and 16-AP probes are located near the surface. Irrespective of the interpretation, the data demonstrated that membranes relax on the ns timescale, but the details are not completely understood.

7.5. PICOSECOND RELAXATION IN SOLVENTS

Advanced Topic

In fluid solvents at room temperature spectral relaxation is usually complete within about 10 ps, which is prior to the emission of most fluorophores. This rapid process is too rapid to be resolved with the usual instrumentation for time-domain or frequency-domain fluorescence. However, advances in laser technology and methods for ultrafast spectroscopy have resulted in an increasing interest in ps and fs solvent dynamics.[49–61] Because of the rapid timescale the data on solvent dynamic are usually obtained using fluorescence upconversion. This method is described in Chapter 4. Typical data are shown in Figure 7.22 for coumarin 152 (C152). The intensity decays very quickly on the blue side of the emission, and displays a rise on the long-wavelength side of the emission. The total intensity decay of coumarin 152 with a lifetime of 0.9 ns is not visible on the ps timescale of these measurements, as is seen as the nearly horizontal line after 1 ps in the lower panel. The wavelength-dependent upconversion data were used to reconstruct the time-resolved emission spectra, which are shown in Figure 7.23 at 0.1 and 5.0 ps. By 5 ps the relaxation is essentially complete, which is why time-dependent effects are usually not considered for fluorophores in fluid solution.

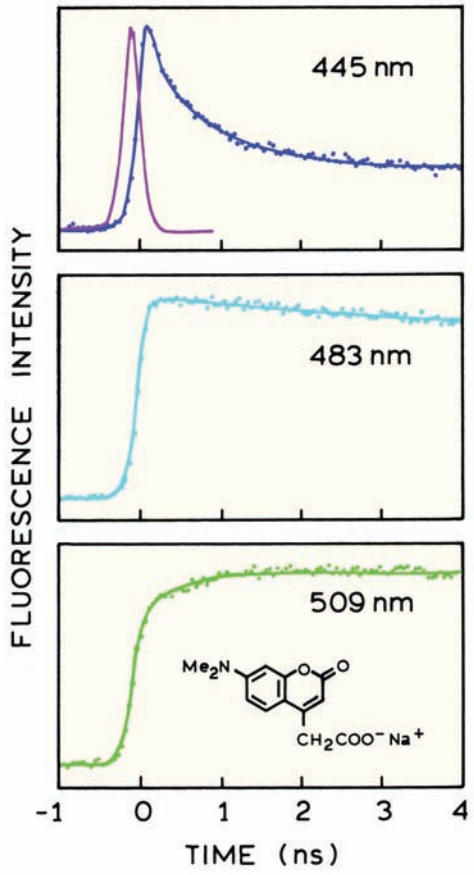

Figure 7.22. Fluorescence upconversion intensity decays of 7-(dimethylamino)coumarin-4-acetate (C152) in water. The solid line through the points is a multi-exponential fit to the intensity decay at each wavelength. The peak near zero time in the upper panel is the instrument response function (280 fs FWHM). Revised and reprinted with permission from [61]. Copyright © 1988, American Chemical Society.

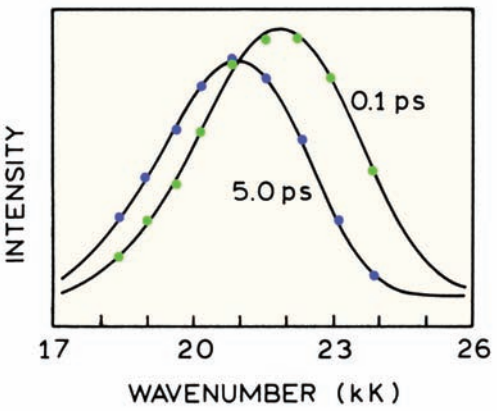

Figure 7.23. Time-resolved emission spectra of 7-(dimethylamino)-coumarin-4-acetate in water at 0.1 and 5.0 ps after excitation. Revised and reprinted with permission from [61]. Copyright © 1988, American Chemical Society.

7.5.1. Theory for Time-Dependent Solvent Relaxation

There is no comprehensive theory that can be used to explain all time-dependent spectral shifts. This is because the spectral shifts can have their molecular origin in general solvent effects, specific solvent effects, or other excited-state processes. However, it is possible to predict the time dependence of spectral shifts due to general solvent effects. The basic idea is that the reaction field around the excited molecule relaxes in a manner predictable from the dielectric relaxation times (τ_D).[62–65] The dielectric relaxation time is a measure of the time needed for solvent molecules to reorient in response to an electric field. However, the spectral relaxation time (τ_S) is not expected to be equal to τ_D, but to be equal to the longitudinal relaxation time (τ_L). The value of τ_L is related to the dielectric relaxation time (τ_D) by

$$\tau_S \simeq \tau_L = \tau_D \frac{2\varepsilon_\infty + \varepsilon_C}{2\varepsilon_0 + \varepsilon_C} \qquad (7.9)$$

where ε_∞ is the infinite frequency dielectric constant, and ε_0 is the low-frequency dielectric constant. The value of ε_c is the dielectric constant of the cavity containing the fluorophore and is usually set equal to 1, which is near the dielectric constant of organic molecules. The values of τ_L are often estimated using various approximations. The value of ε_∞ is often taken as n^2, where n is the refractive index, and the value of ε_0 is taken as the static dielectric constant ε. Expressions used for τ_L include[66–69]

$$\tau_S \simeq \tau_L = \frac{2n^2 + 1}{2\varepsilon + 1}\tau_D \simeq \frac{\varepsilon_\infty}{\varepsilon_0}\tau_D \simeq \frac{n^2}{\varepsilon}\tau_D \qquad (7.10)$$

Values of τ_D and τ_L for typical solvents are given in Table 7.2. For polar solvents the spectral relaxation times are expected to be five- to tenfold smaller than the value of τ_D. Hence the rate of spectral relaxation is expected to be faster than the rate of dielectric relaxation.

At first glance it seems that the spectral relaxation time should be equal to the dielectric relaxation time, which depends on the rotational rate of the fluorophore. It appears that the difference between τ_D and τ_S can be explained by classical electrodynamics.[62] The value of τ_D refers to the rate of reorientation of the fluorophores to a fixed voltage. Experimentally a fixed voltage is placed on a capacitor at $t = 0$, and this voltage is maintained while the system relaxes. The solvent relaxation time is more consistent with creation of a fixed charge on the capacitor at $t = 0$, with no additional current flow during relaxation. This second type of experiment predicts the relationship between τ_S and τ_D in eq. 7.9.

Unfortunately, solvent relaxation even in simple solvents is expected to be complex. This is because most solvents are known to display multiple dielectric relaxation times. For instance, propanol is known to display three dielectric relaxation times. Typical values are listed in Table 7.3. The largest value (τ_{D1}) is too large for overall rotation

Table 7.2. Dielectric Properties of Solvents

Solvent	°C	ε_0	ε_∞	n	τ_D (ps)	τ_L (ps)	Ref.
Water	25	78.3	5.2	1.33	8.3	0.4	70
Methanol	19	31.8	2.0	1.33	60	8.2	71
Ethanol	19	26.0	1.9	1.36	90	12.4	71
n-Propanol	19	21.3	1.9	1.38	320	59 ps	71
	–20	27	5.6	–	1.3 ns	0.34 ns	72–74
Glycerol	12	46.8	4.0	–	39 ps	–	75
	–70	74	4.2	–	0.11 ns	–	73

Table 7.3. Dielectric Relaxation Times of Alcohols[76–77]

	°C	τ_{D1} (ps)	τ_{D2} (ps)	τ_{D3} (ps)
Methanol	20	52	13	1.4
Ethanol	20	191	16	1.6
n-Propanol	20	430	22	2
	40	286	17	2
n-Butanol	20	670	27	2.4
n-Octanol	20	1780	38	3
	40	668	29	3

of the alcohol molecules, and is attributed to rotation of the alcohol following breakage of a hydrogen bond. The second dielectric relaxation time (τ_{D2}) is assigned to rotational diffusion of the free alcohol molecule. The shortest time (τ_{D3}) is assigned to rotation of the hydroxyl group around the carbon-oxygen bond. Based on this behavior, the center of gravity of the emission spectrum of a fluorophore in n-propanol is expected to decay as

$$\bar{\nu}_{cg}(t) = \bar{\nu}_\infty + (\bar{\nu}_0 - \bar{\nu}_\infty) \sum_i \beta_i \exp(t/\tau_{Si}) \quad (7.11)$$

where β_i are the amplitudes associated with each relaxation time (τ_{si}). Hence, the time-dependent values of $\bar{\nu}_{cg}(t)$ can show complex multi-exponential decays even in simple solvents. Complex decays of $\bar{\nu}_{cg}(t)$ were already seen for a labeled protein in Figure 7.11.

Spectral relaxation data are frequently presented as the correlation function

$$C(t) = \frac{\bar{\nu}_{cg}(t) - \bar{\nu}_\infty}{\bar{\nu}_0 - \bar{\nu}_\infty} \quad (7.12)$$

This expression has the advantage of normalizing the extent of relaxation to unity, allowing different experiments to be compared. However, when using eq. 7.12, one loses the information on the emission spectra at $t = 0$ and $t = \infty$. If some portion of the relaxation occurs more rapidly than the time resolution of the measurement, this portion of the energy will be missed and possibly not noticed.

7.5.2. Multi-Exponential Relaxation in Water

It is of interest to understand the relaxation times expected for probes in water. Such experiments have become possible because of the availability of femtosecond lasers. One such study examined 7-(dimethylamino)coumarin-4-acetate in water (Figure 7.22).[61] The excitation source was a styryl 8 dye laser, with a 1,1',3,3,3',3'-hexamethylindotricarbocyanine iodide (HITCI) saturable absorber, which provided 70-fs pulses at 792 nm. These pulses were frequency doubled for excitation at 396 nm.

The emission was detected using sum frequency upconversion with a potassium dehydrogen phosphate (KDP) crystal and the residual 792-nm light for gating the crystal. The instrument response function with an FWHM of 280 fs allowed the intensity decay to be directly recorded (Figure 7.22). These decays showed a rapid component on the short-wavelength side of the emission (top panel), a nearly single-exponential decay near the middle of the emission spectrum (middle panel), and a rise time on the low-energy side of the emission (bottom panel).

These upconversion data allowed construction of the TRES. The time-dependent shifts all occur within 5 ps (Figure 7.24). In this case it was necessary to use two correlation times of 0.16 and 1.2 ps to account for the time-dependent shifts. Both values are smaller than the dielectric relaxation time of water, which is near 8.3 ps (Table 7.2). Similar results have been observed for other fluorophores in other solvents. In general, spectral relaxation times are shorter than the τ_D values, but the values of τ_S can be smaller or larger than the calculated values of τ_L. This is illustrated by Yt-base in n-propanol at –20°C.[78] At least two relax-

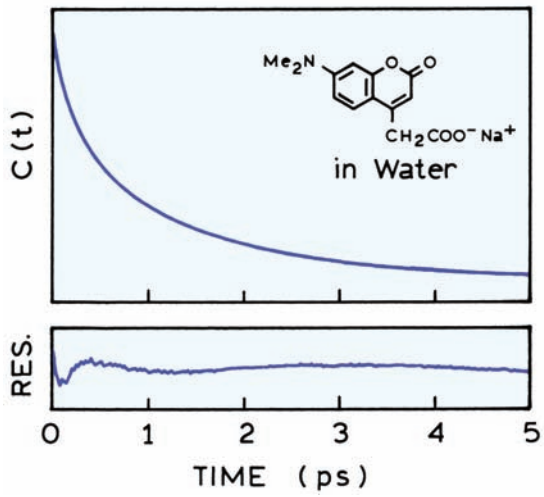

Figure 7.24. Correlation function for spectral relaxation of 7-(dimethylamino)coumarin-4-acetate in water. The upper section of the figure is a superposition of an experimentally determined $C(t)$ function for the water and a biexponential function with relaxation time of 0.16 and 1.2 ps. The lower panel shows the residuals for this fit expanded threefold. Revised and reprinted with permission from [61]. Copyright © 1988, American Chemical Society.

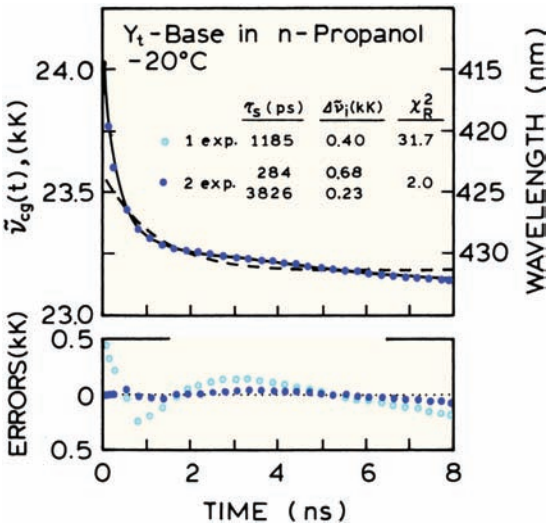

Figure 7.25. Time-resolved emission center of gravity of Yt-base in n-propanol at –20°C. From [78].

ation times are required to explain the time-dependent shifts (Figure 7.25). One can use the correlation functions $C(t)$ to compare the measured and expected relaxation times (Figure 7.26). For Yt-base in propanol the decay of C(t) is faster than predicted from the dielectric relaxation time τ_D, and slower than predicted from the longitudinal relaxation time

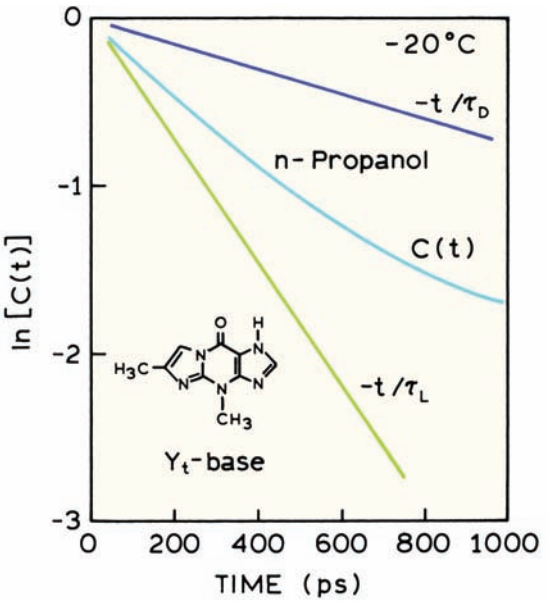

Figure 7.26. Extent of spectral relaxation for Yt-base [$C(t)$], compared to the dielectric (τ_D) and longitudinal (τ_L) relaxation times of n-propanol at –20°C. Revised from [78].

τ_L. This result is typical of that observed for many fluorophores in polar solvents.[79]

7.6. MEASUREMENT OF MULTI-EXPONENTIAL SPECTRAL RELAXATION

Measurement of the complete process of spectral relaxation is a technological challenge. Such measurements are difficult because relaxation occurs over a wide range of timescales. For instance, the dielectric relaxation times for a simple solvent like n-octanol range from 3 to 1780 ps (Table 7.3). Hence the apparatus needs to have resolution of both ps and ns processes. As discussed in Chapter 4,

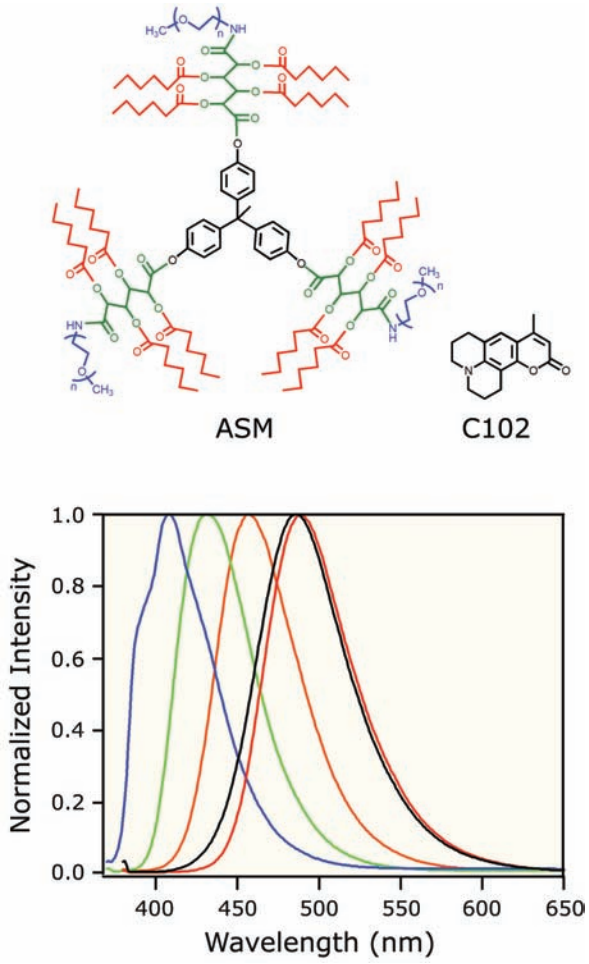

Figure 7.27. Chemical structures of an amphiphilic starlike macromolecule (ASM) and coumarin 102 (C102). The lower panel shows the emission spectra of C102 in cyclohexane (blue), ethyl acetate (green), octanol (orange), water (red) and bound to the ASM in water (black). Reprinted with permission from [80]. Copyright © 2002, American Chemical Society. Courtesy of Dr. Edward W. Castner, Jr. from the Rutgers University, NJ.

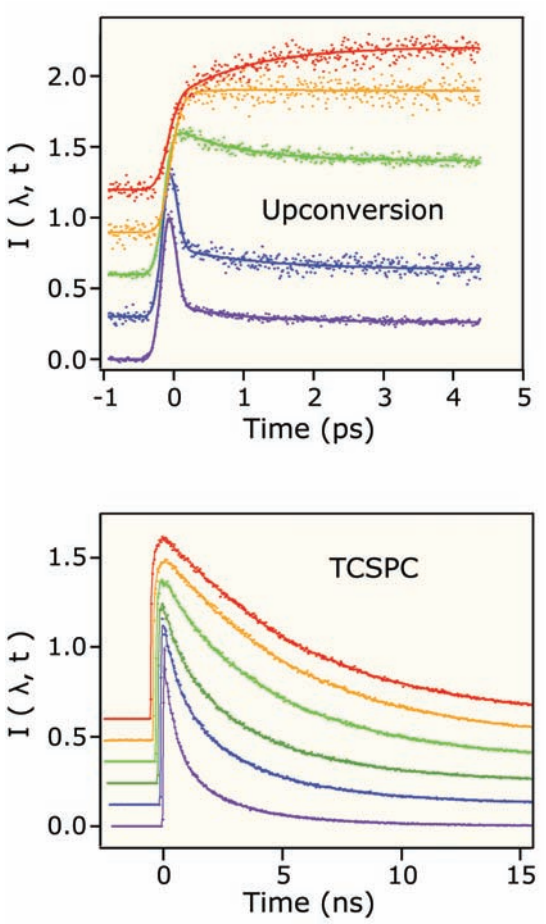

Figure 7.28. Wavelength-dependent intensity decays of C102 bound to the ASM. Top, fluorescence upconversion. Bottom, TCSPC. Revised and reprinted with permission from [80]. Copyright © 2002, American Chemical Society. Courtesy of Dr. Edward W. Castner, Jr. from the Rutgers University, NJ.

TCSPC can measure decay time down to about 50 ps. Fluorescence upconversion can be used to measure subpicosecond decay times but is generally less useful for decay times above 100 ps. Hence it would be difficult to measure spectral resolution in a solvent like n-octanol using either type of instrument.

An instructive approach to measuring multi-exponential spectra relaxation is provided for coumarin 102 (C102) bound to an amphiphilic starlike macromolecules (ASM). Such molecules are being developed for use as nanoscale drug carriers. A typical ASM contains a lipophilic core to bind nonpolar drugs and a hydrophilic outer shell for water solubility (Figure 7.27). Such molecules are more stable than other carriers such as micelles or liposomes. The emission spectra of C102 is highly sensitive to solvent polarity. The emission spectrum of C102 bound to the ASM shows that C102 is highly sensitive to solvent polarity, and that C102 is located in a polar water-like environment.[80] The similarity of the emission spectra of C102 in water and in the ASM solution suggests that C102 is in the aqueous phase. However, the anisotropy decays (not shown) demonstrated that C102 was mostly bound to the ASM.

Figure 7.28 shows the wavelength-dependent intensity decays of C102 bound to the ASM. The top panel shows decays measured using fluorescence upconversion for times from 0 to 5 ps. The lower panel shows decays measured by TCSPC for times up to 15 ns. As expected for spectral relaxation, the intensity decayed more rapidly on the short-wavelength side of the emission. These decays were used to calculate the time-relaxed emission spectra (Figure 7.29). Relaxation is occurring both on a subpicosecond timescale, and on a timescale near 500 ps. Using TCSPC measurements alone would have probably not detected the subpicosecond component.

7.7. DISTINCTION BETWEEN SOLVENT RELAXATION AND FORMATION OF ROTATIONAL ISOMERS

The shape of the TRES can yield insights into the molecular origin of the time-dependent spectral changes.[81] This concept is illustrated by studies of two closely related fluorophores (BABAPH and BABP, Figure 7.30). These dyes have been used as probes of membrane potential, but an understanding of their excited-state properties was not available. These dyes are known to be solvent dependent, but there was also the possibility that BABP formed rotational isomers in the excited state. In order to separate the solvent-dependent spectral shifts from formation of a polar twisted rotamer, two closely related molecules were examined. The BABAPH derivative contains an ethylene bridge that prevents rotation of the dibutylamino group in the ground or excited state.

Time-resolved decays were recorded at single wavelengths and the decays analyzed in terms of the multi-exponential model. These decays were then used to calculate the time-resolved emission spectra. The normalized TRES show that BABP displays a larger time-dependent shift than does the restrained analogue BABAPH (Figure 7.31). Importantly, the shape of the TRES were time dependent for BABP, but were independent of time for BABAPH. This result was interpreted in terms of formation of a polar twisted state for BABP. Formation of the twisted state was also

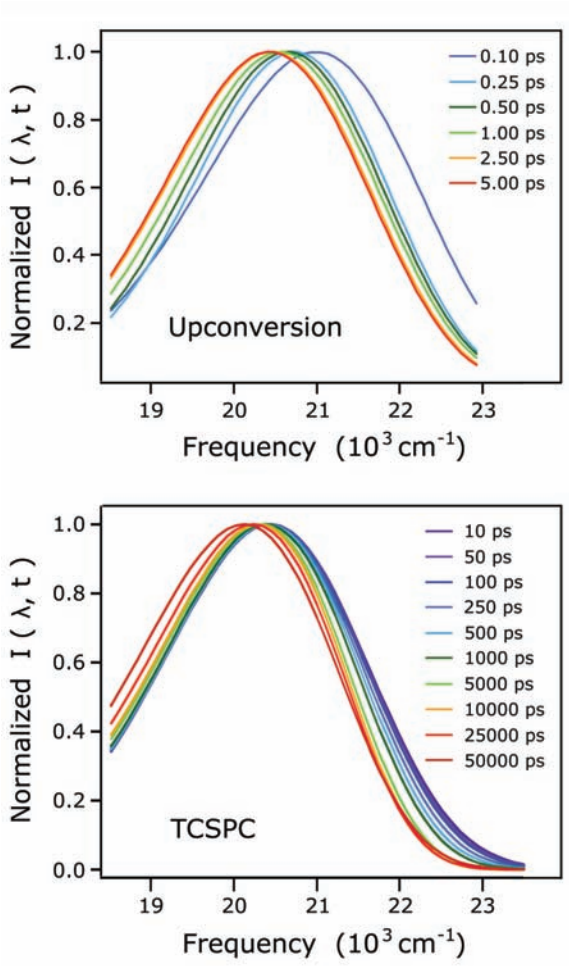

Figure 7.29. Time-resolved emission spectra of ASM encapsulated C102. Top, fluorescence upconversion. Bottom, TCSPC. Revised and reprinted with permission from [80]. Copyright © 2002, American Chemical Society. Courtesy of Dr. Edward W. Castner, Jr. from the Rutgers University, NJ.

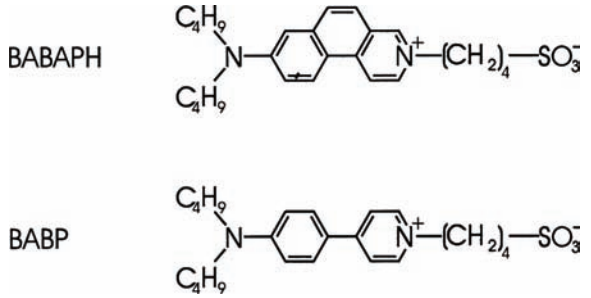

Figure 7.30. Hemicyanine dyes 2-(sulfonatobutyl)-7-(dibutylamino)-2-azaphenanthrene (BABAPH) and 1-(sulfonatobutyl)-4-[4'-(dibutylamino)phenyl]pyridine (BABP). Reprinted with permission from [81]. Copyright © 1996, American Chemical Society.

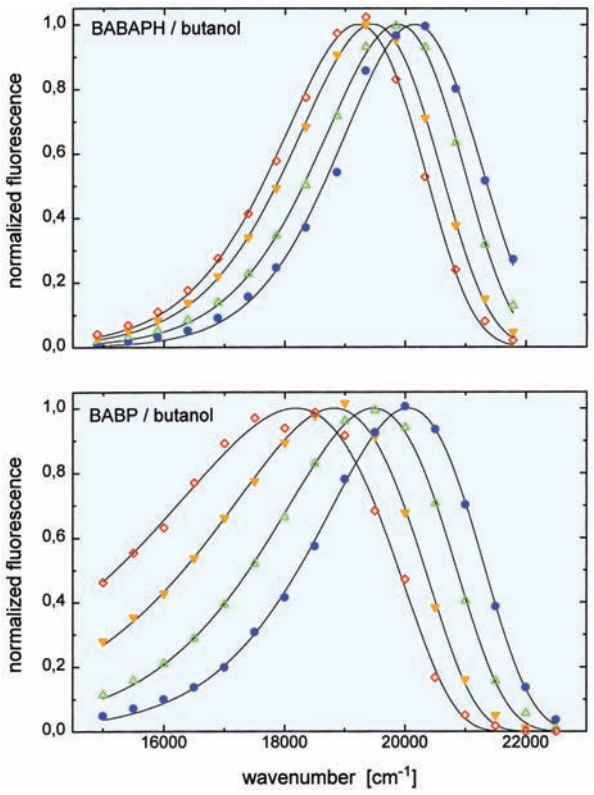

Figure 7.31. Normalized time-resolved emission fluorescence spectra of BABAPH and BAPH in butanol, 25°C, at time delays of 20, 50, 150, and 2000 ps after excitation (from right to left). The data are fitted by the log-normal spectral-shape functions. Reprinted with permission from [81]. Copyright © 1996, American Chemical Society.

an additional rate of deactivation, resulting in more rapid intensity decays for BABP than for BABAPH (Figure 7.32, lower panel).

The TRES were also used to determine the time-dependent center of gravity ($\bar{\nu}_{cg}(t)$) and the time-dependent half width ($\Delta\bar{\nu}_{cg}(t)$). The results of least-squares fitting of the TRES line shapes are shown in Figure 7.32. The dramatic difference in spectral shape between BABP and BABAPH is seen in the middle panel. The spectral width of the restrained analogue BABP is independent of time, whereas BABAPH shows an increase in spectral width. The data are consistent with rotation of the dibutylamino group in BABP to allow a larger charge separation than in BABAPH. The larger charge separation results in a new species emitting at longer wavelengths, and thus the increase in spectral half width of BABAPH. In this case the TRES provided an explanation for the different spectral shifts displayed by these similar molecules.

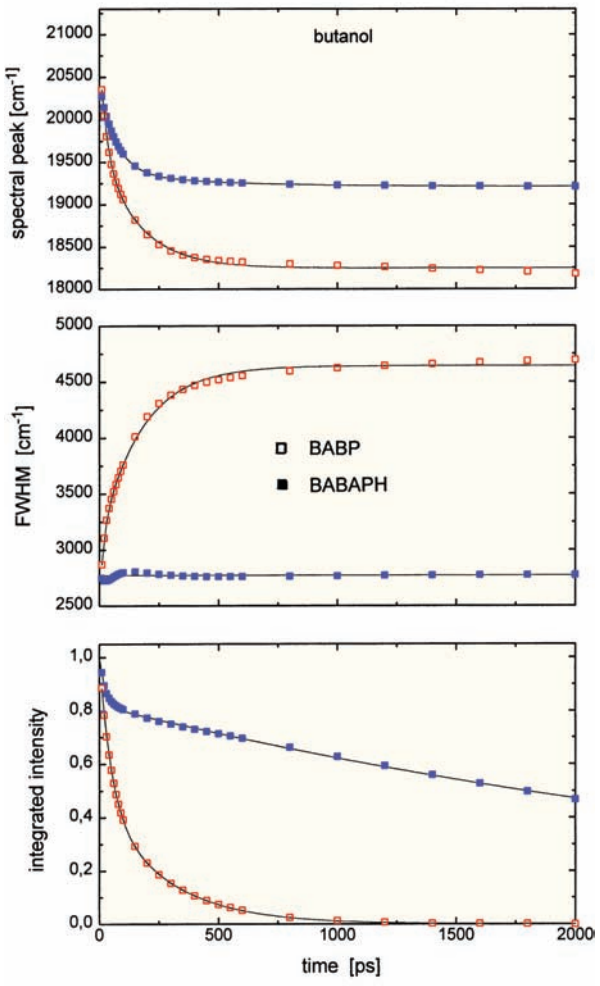

Figure 7.32. Fluorescence dynamics of BABAPH (full symbols) and BABP (open symbols) in butanol at 25°C. Top: Position of spectral maximum. Middle: Spectral width (full width at half maximum). Bottom: Integral intensity normalized to its initial value. Reprinted with permission from [81]. Copyright © 1996, American Chemical Society.

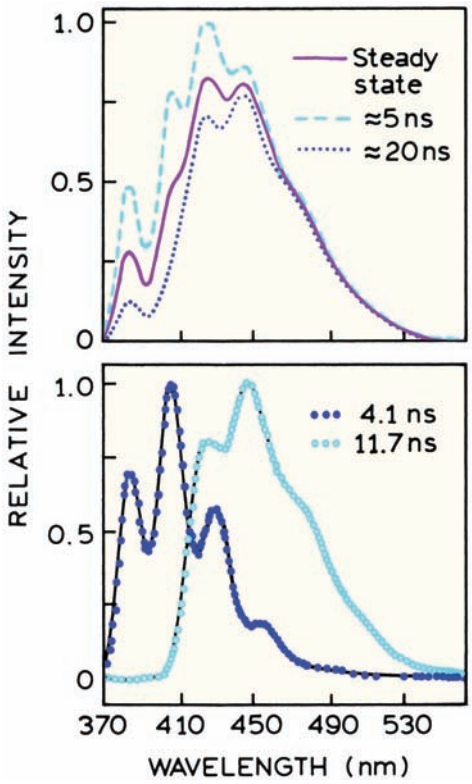

Figure 7.33. **Top**: Steady-state (solid curve) and time-resolved emission spectra of a mixture of anthracene and 9-cyano-anthracene. The TRES are shown for an early time window near 5 ns and a late time window near 20 ns. **Bottom**: Decay-associated spectra: 4.1 ns (dotted) and 11.7 ns (○). components. Revised and reprinted with permission from [82]. Copyright © 1982, American Chemical Society.

7.8. COMPARISON OF TRES AND DECAY-ASSOCIATED SPECTRA

In Chapters 4 and 5 we described the use of time-resolved data to calculate the decay-associated spectra (DAS). One may ask how the DAS are related to the TRES. There is no direct relationship between these two types of calculated spectra. This can be seen by examination of the TRES and DAS for a mixture of fluorophores (Figure 7.33, top). This mixture contained anthracene (τ = 4.1 ns) and 9-cyanoanthracene (9-CA, τ = 11.7 ns).[82] The TRES show contributions from anthracene and 9-CA at all times. At shorter times (approximately 5 ns) the contribution from anthracene is larger than in the steady-state spectrum. At longer times (approximately 20 ns) the relative contribution of the shorter-lived anthracene becomes smaller.

The DAS for this mixture have a completely different meaning (Figure 7.33, bottom). These calculated spectra correspond to the emission spectra of the individual components. Also, the DAS are not dependent on time. Interpretation of the DAS is straightforward for a mixture of fluorophores. However, for time-dependent spectral relaxation the DAS can be positive or negative, and hence do not correspond to the emission spectra of any particular component.

7.9. LIFETIME-RESOLVED EMISSION SPECTRA

Advanced Topic

In the preceding sections we described the relatively complex experiments needed to calculate time-resolved emis-

sion spectra. In some circumstances it is possible to obtain information about the rate of relaxation using only steady-state measurements. The basic idea is to use collisional quenching to decrease the lifetime of the excited state (τ) to a value comparable to the relaxation time (τ_S). As described in Section 7.5, the center of gravity of the emission can be expected to decay exponentially from $\bar{\nu}_0$ at $t = 0$ to ν_∞ at $t = \infty$ according to

$$\bar{\nu}_{cg}(t) = \bar{\nu}_\infty + (\bar{\nu}_0 - \bar{\nu}_\infty) \exp(-t/\tau_S) \tag{7.13}$$

Suppose the total intensity decays with a single decay time τ. The center of gravity observed in a steady-state emission spectra is given by the integral average of $\bar{\nu}_{cg}(t)$ over the intensity decay:

$$\bar{\nu}_{cg} = \frac{\int_0^\infty \bar{\nu}_{cg}(t) \exp(-t/\tau)\, dt}{\int_0^\infty \bar{\nu}_{cg}(t)\, dt} \tag{7.14}$$

Substitution of eq. 7.13 into 7.15 yields

$$\bar{\nu}_{cg} = \bar{\nu}_\infty + (\bar{\nu}_0 - \bar{\nu}_\infty)\frac{\tau_S}{\tau_S + \tau} \tag{7.15}$$

This expression connects the center-of-gravity observed in a steady-state experiment, with the relative values of the decay time τ and the spectral relaxation time τ_S. From this expression one can also understand the spectral shifts observed at low and high temperatures. At low temperature, $\tau_S >> \tau$, and the center of gravity is $\bar{\nu}_0$. At high temperature, $\tau_S << \tau$, and the relaxed emission is observed. The center of gravity and/or emission spectrum is sensitive to temperature or lifetime when $\tau_S \simeq \tau$.

Examination of eq. 7.15 suggests an alternative way to measure spectral relaxation.[83–85] Suppose the lifetime τ can be changed. Then $\bar{\nu}_{cg}$ will vary depending on the relative values of τ and τ_S. One way to vary the lifetime is by collisional quenching. In the presence of a quenching agent the fluorescence lifetime is decreased according to

$$\tau = \tau_0/(1 + K_D[Q]) \tag{7.16}$$

where τ_0 is the lifetime in absence of quenching, K_D is the collisional quenching constant, and $[Q]$ is the concentration of quencher. Strictly speaking, calculation of τ in the presence of quencher requires the separation of the static and dynamic quenching constants. Hence, the dynamic quenching constant (K_D, Chapter 8) should be used when calculating the lifetime. For significant quenching one requires solutions of relatively low viscosity to permit rapid diffusion of the quencher. The quenching procedure is particularly useful for biological macromolecules. This is because it permits the relaxation rates to be measured without variation of the temperature. For proteins and membranes, such temperature changes can themselves alter the relaxation rates. An additional advantage of lifetime-resolved measurements is that only steady-state measurements are required, assuming τ_0 and K_D are known.

Lifetime-resolved emission spectra of TNS-labeled vesicles are illustrated in Figure 7.34. In this case oxygen was used to decrease the lifetime of TNS. As the average lifetime is decreased from 6.7 to 0.53 ns, the steady-state spectra are seen to shift almost 20 nm to shorter wavelengths. Quenching of fluorescence is a random collisional encounter between TNS and the oxygen molecule. Those fluorophores that remain in the excited state for a longer period of time are more likely to be quenched. The longer-lived fluorophores are also those for which relaxation is more complete. Quenching selectively prevents observation of the emission from these more relaxed fluorophores, and thus results in shifts of the average emission to shorter wavelengths. The lack of change in spectral shape is consistent with the continuous relaxation process shown in Figure 7.6.

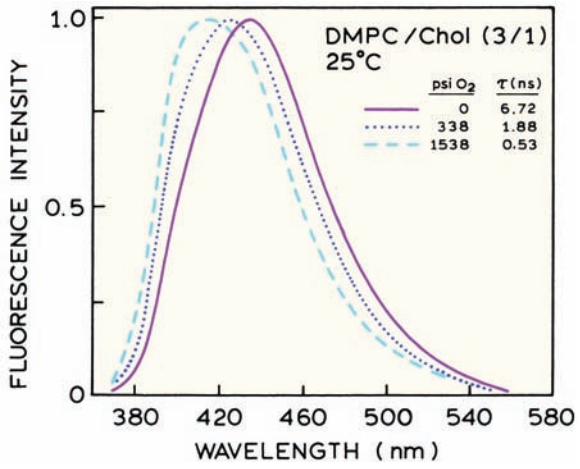

Figure 7.34. Effects of oxygen quenching on the fluorescence emission spectrum of TNS-labeled DMPC/cholesterol (3:1) vesicles. Reprinted with permission from the American Chemical Society. Revised and reprinted with permission from [85]. Copyright © 1981, American Chemical Society.

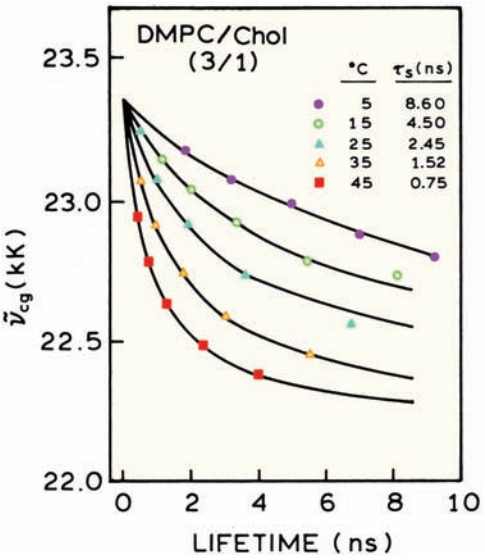

Figure 7.35. Lifetime-resolved centers of gravity for TNS-labeled DMPC/cholesterol vesicles. Revised and reprinted with permission from [85]. Copyright © 1981, American Chemical Society.

These lifetime-dependent spectra can be used to measure the spectral relaxation times at the DMPC/cholesterol membranes over a range of temperatures (Figure 7.35). The solid lines through the datapoints represent the best fit using eq. 7.15. It is interesting to note that all these relaxation times fall into a narrow range from 8.6 to 0.75 ns, and do not show evidence for a phase transition. This is probably because the TNS is localized at the lipid–water interface, when the dynamic properties are similar irrespective of the phase state of the acyl side chains.

Oxygen quenching of fluorescence is particularly useful for lifetime-resolved studies of solvent relaxation. Oxygen quenching can provide a wide range of lifetimes with little change in solvent composition. This is because oxygen diffuses rapidly in most solvents, and it is a small nonpolar molecule. In addition, oxygen is highly soluble in organic solvents and is an efficient collisional quencher. These properties result in a large accessible range of lifetimes. However, oxygen quenching requires specialized pressure cells,[83] and of course there are dangers when using high pressures and/or organic solvents.

7.10. RED-EDGE EXCITATION SHIFTS

Advanced Material

In all the preceding discussions we assumed that the emission spectra were independent of the excitation wavelength.

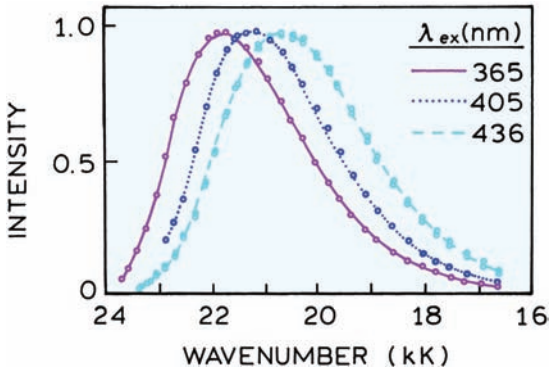

Figure 7.36. Emission spectra of 3-amino-N-methylphthalimide in isobutanol at –100°C. The sample was excited at 365 nm (solid), 405 nm (dotted), and 436 nm (dashed). At 20°C all excitation wavelengths yielded the same emission spectrum (dashed). Revised from [91].

This is a good assumption for fluorophores in fluid solvents. However, this assumption is no longer true in viscous and moderately viscous solvents. For polar fluorophores under conditions where solvent relaxation is not complete, emission spectra shift to longer wavelengths when the excitation is on the long-wavelength edge of the absorption spectrum. This effect can be quite substantial, as is shown for 3-amino-N-methylphthalimide in Figure 7.36. This is known as a red-edge excitation shift, which has been observed in a number of laboratories for a variety of fluorophores.[86–97]

What is the origin of this unusual behavior? The behavior of polar molecules with red-edge excitation can be understood by examining a Jablonski diagram that includes spectral relaxation (Figure 7.37). Suppose the fluorophore is in a frozen solvent, and that the sample is excited in the center of the last absorption band (λ_C) or on the red edge (λ_R). For excitation at λ_C the usual emission from the *F* state is observed; however, excitation at λ_R selects for those fluorophores that have absorption at lower energy. In any population of molecules in frozen solution there are some fluorophores that have a solvent configuration similar to that of the relaxed state. These fluorophores are typically more tightly hydrogen bonded to the solvent, and thus display a red-shifted emission. In frozen solution the fluorophore-solvent configuration persists during the intensity decay, so that the emission is red shifted.

Knowing the molecular origin of the red-edge shifts, it is easy to understand the effects of increasing temperature. It is known that the red-edge shift disappears in fluid solvents. This is because there is rapid reorientation of the solvent. Hence, even if red-emitting fluorophores are initially

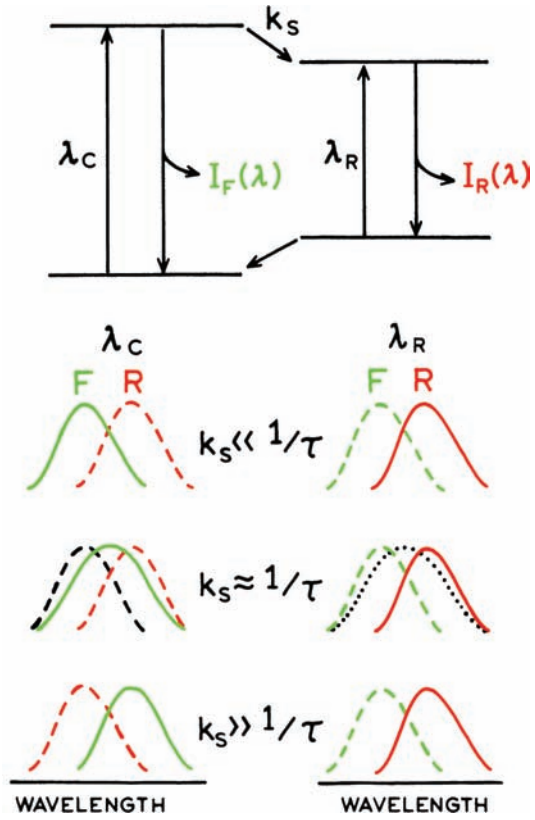

Figure 7.37. Effects of red-edge excitation on emission spectra. The term λ_C indicates excitation in the center of the last absorption band of the fluorophore. The term λ_R indicates excitation on the red edge of the absorption band. The solid lines represent the observed spectra. To allow comparison the dashed lines represent the emission spectra of either the *F* or *R* state. The dotted line (middle panel) represents a possible consequence of reverse relaxation. Revised and reprinted with permission from [98]. Copyright © 1984, American Chemical Society.

excited, the emission spectra reach equilibrium prior to emission. This implies that there may be some reverse relaxation from the red-shifted emission to the equilibrium condition, as is shown in the middle panel for $k_S \simeq \tau^{-1}$ (Figure 7.37). In fact, relaxation to higher energies has been observed with red-edge excitation.

Red-edge excitation has been applied to biochemically relevant fluorophores. The widely used probe 1,8-ANS displays a substantial red shift (Figure 7.38). As the excitation wavelength is increased, the emission maxima converge to the same value typical of the relaxed emission (Figure 7.39). This suggests that excitation red shift can be used to estimate biopolymer dynamics.[98–100] Excitation red shifts should only be observed if relaxation is not complete. Also, the magnitude of the red shifts will depend on the rate of

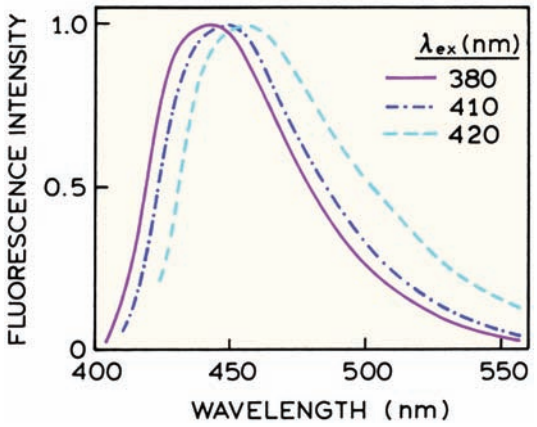

Figure 7.38. Fluorescence emission spectra 8-anilinonaphthalene-1-sulfonic acid in 1-propanol at 77°K. Excitation and emission bandpass are both 5 nm. Revised from [95].

spectral relaxation. Excitation red shifts have been observed for labeled proteins, labeled membranes,[101–104] and for the intrinsic tryptophan fluorescence of proteins.[105–109]

7.10.1. Membranes and Red-Edge Excitation Shifts

Red-edge excitation shifts (REES) are displayed by solvent sensitive fluorophores in polar environments. This suggests the use of REES to study fluorophores that localize in the headgroup region of lipid bilayers. One example is shown in Figure 7.40 for adducts of NBD. Two NBD derivatives were used: NBD-PE and NBD-Cholesterol. It seemed likely that the polar NBD groups would localize at the lipid–water interface, especially below the phase transition temperature of the DPPC vesicles where the acyl side

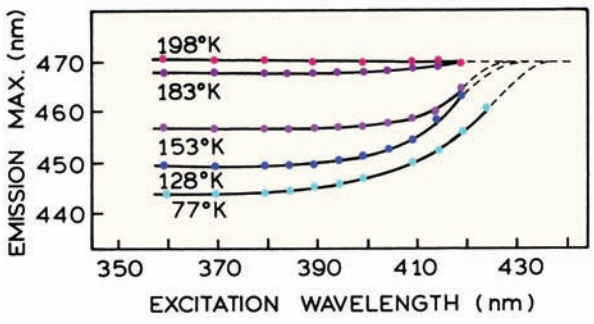

Figure 7.39. Temperature dependence of fluorescence excitation red shift for 8-anilinonaphthalene-1-sulfonic acid in 1-propanol. Revised from [95].

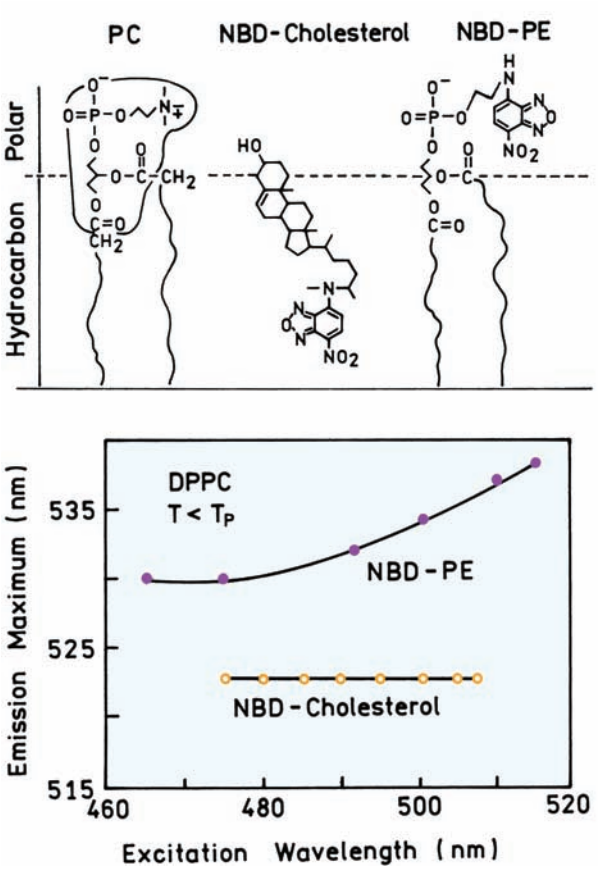

Figure 7.40. Red-edge excitation shifts for NBD-PE and NBD-cholesterol in gel phase DPPC vesicles. Revised from [102].

chains are in an ordered conformation. The lower panel in Figure 7.40 shows the dependence of the emission maximum on the excitation wavelengths. For NBD-PE the emission maxima shift about 8 nm with red-edge excitation. In contrast, the emission maxima of NBD cholesterol remain constant regardless of the excitation wavelength. The absence of an REES and the short-wavelength emission maxima of NBD-cholesterol indicate that the NBD group is localized in the acyl side chain region of the membrane, as shown in Figure 7.40. Apparently, the forces that orient the cholesterol moiety are large enough to overcome the tendency of the polar NBD group to localize at the lipid–water interface.

7.10.2. Red-Edge Excitation Shifts and Energy Transfer

Red-edge excitation shifts can explain some unusual observations. There are early reports that suggested the failure of homoresonance energy transfer on red-edge excitation.[110–112] These studies also reported a decrease in the rate of rotational diffusion upon red-edge excitation. The smaller rate of rotational diffusion was explained as being due to excitation of an out-of-plane transition that was not capable of RET. In retrospect, these data are all understandable in terms of the red-edge effect shown in Figure 7.37. The decrease in homotransfer was probably due to the spectral shifts that decreased the overlap integral for homotransfer. The decrease in the rate of rotation can be explained as due to increased hydrogen bonding to the solvent. It is known that the rate of rotational diffusion decreases with increasing numbers of fluorophore-solvent hydrogen bonds.[113] Hence, shifts in the emission spectra can explain the failure of RET with red-edge excitation.

7.11. EXCITED-STATE REACTIONS

In the preceding sections of this chapter we considered the interactions of fluorophores with their surrounding environment. These interactions did not involve chemical reactions of the fluorophores. However, fluorophores can undergo chemical reactions while in the excited state. Such reactions occur because light absorption frequently changes the electron distribution within a fluorophore, which in turn changes its chemical or physical properties. The best-known example of a fluorophore that undergoes an excited-state reaction is phenol. In neutral solution phenol and naphthols can lose the phenolic proton in the excited state. Deprotonation occurs more readily in the excited state because the electrons on the hydroxyl groups are shifted into the aromatic ring, making this hydroxyl group more acidic. Excited-state reactions are not restricted to ionization. Many dynamic processes that affect fluorescence can be interpreted in terms of excited-state reactions. These processes include resonance energy transfer and excimer formation (Table 7.4). Excited-state processes display characteristic time-dependent decays that can be unambiguously assigned to the presence of an excited-state process.

Perhaps the most dominant type of an excited-state reaction in the loss or gain of protons.[114–124] Whether a fluorophore loses or gains a photon in the excited-state reaction is determined from the direction of the change in pK_A in the excited state. If the pK_A decreases ($pK_A^* < pK_A$), where the asterisk denotes the excited state, then the fluorophore will tend to lose a proton in the excited state. If the pK_A increases ($pK_A^* > pK_A$), then the fluorophore may pick up a proton in the excited state. The best known examples

Table 7.4. Known Excited-State Ionization Reactions

Reaction	Compound	pK_A	pK_A^*	D or P[a]
$ROH \leftrightarrows RO^- + H^+$	Phenol	10.0	4.1	D
	1-Naphthol	9.2	2.0	D
	2-Naphthol	9.5	2.8	D
	HPTS[b]	7.3	1.0	D
$RNH_2 \leftrightarrows RNH^- + H^+$	2-Naphthylamine	>14	12.2	D
$RNH_3^+ \leftrightarrows RNH_2 + H^+$	2-Naphthylamine H^+	4.1	–1.5	D
$ArN + H^+ \leftrightarrows ArNH^+$	Acridine	5.1	10.6	P
$RCO_2^- + H^+ \leftrightarrows RCO_2H$	Benzoic acid	4.2	9.5	P
	1-Naphthoic acid	3.7	7.7	P
	Anthracene-9-carboxylic acid	3.7	6.9	P

[a]Deprotonation (D) or protonation (P).

[b]HPTS, 8-hydroxypyrene-1,3,6-trisulfonate.

are phenols and acridines. In general, phenols undergo excited-state deprotonation, and acridine undergoes excited-state protonation. Electron donors such as –OH, –SH, $–NH_2$ have a lone pair of electrons, and these electrons tend to become more conjugated to the aromatic ring system in the excited state, resulting in $pK_A^* < pK_A$. Electron acceptors such as $–CO_2^-$ and $–CO_2H$ have vacant π orbitals into which electrons can be transferred in the excited state. This increased electron density results in weaker dissociation in the excited state: $pK_A^* > pK_A$. Representative ground-state and excited-state pK_As are given in Table 7.4.

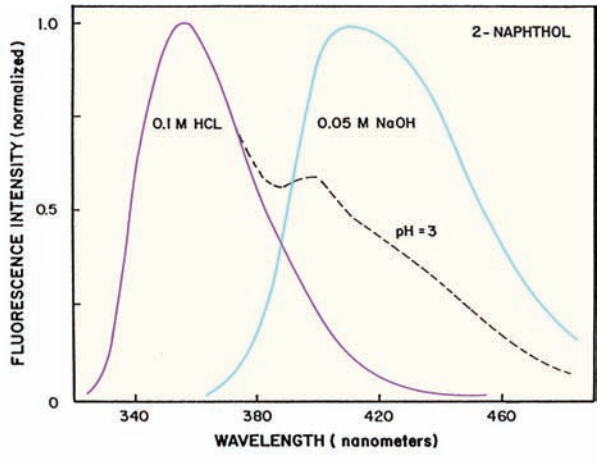

Figure 7.41. Steady-state emission spectra of 2-naphthol. Spectra at 24°C are shown in 0.1 M HCl, 0.05 M NaOH and in water at pH = 3.0 (dashed). Reprinted from [139]. Copyright © 1982, with permission from Elsevier Science.

7.11.1. Excited-State Ionization of Naphthol

Perhaps the most widely studied excited-state reaction is the ionization of aromatic alcohols.[125–131] In the case of 2-naphthol the pK_A decreases from 9.2 in the ground state to 2.0 in the excited state.[130] In acid solution the emission is from naphthol with an emission maximum of 357 nm (Figure 7.41). In basic solution the emission is from the naphtholate anion, and is centered near 409 nm. At intermediate pH values emission from both species is observed (dashed). Depending on pH, the excited-state dissociation of 2-naphthol can be either reversible or irreversible. At pH values near 3 the reaction is reversible, but at pH values above 6 the reaction is irreversible.[129–130] Hence, this system illustrates the characteristics of both reversible and irreversible excited-state reactions.

The spectra shown in Figure 7.41 illustrate another feature of an excited-state process, which is the appearance of the reaction product under conditions where no product is present in the ground state. At low or high pH, the ground-state fluorophore is present in only one ionization state and only the emission from this state is observed. The absorption spectra of these low- and high-pH solutions are characteristic of naphthol and naphtholate, respectively (Figure 7.42). However, at pH = 3 about 50% of the total emission is from each species. Because the ground state pK_A of 2-naphthol is 9.2, only the unionized form is present at pH = 3, and the absorption spectrum is that of unionized naphthol. Whereas only unionized naphthol is present in the ground state at pH 3, the emission spectrum at pH 3 shows emission from both naphthol and naphtholate. At pH 3 the naphtholate emission results from molecules that have

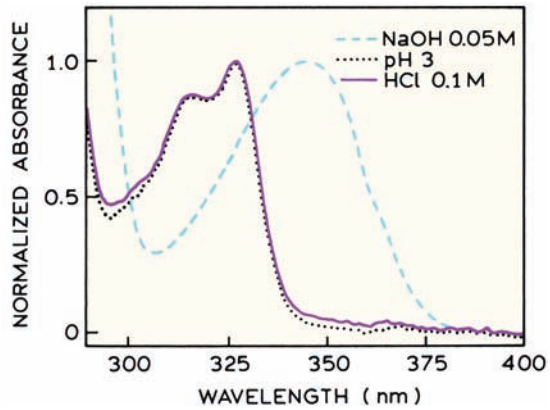

Figure 7.42. Absorption spectra of 2-naphthol in 0.1 M HCl, 0.05 M NaOH, and at pH 3.

undergone dissociation during the duration of the excited state. The invariance of the absorption spectrum, under conditions where the emission spectrum of a reacted state is observed, is a characteristic feature of an excited-state reaction.

This characteristic of an excited-state reaction is shown in Figure 7.43. Suppose one measured the fraction of the signal, absorption or emission, from unionized 2-naphthol. The absorption measurement would show a decrease in this fraction at pH 9.2, which is near the ground state pK_A. The fluorescence measurements would show a change near pH 2, near the pK_A* value of the excited state. The difference is due to ionization that occurs during the excited-state lifetime. Depending on the fluorophore and solvent, the excited-state reaction can be complete or only partially complete during the excited-state lifetime. It is also important to note that the extent of dissociation depends on the buffer concentration. For instance, suppose that 2-naphthol is dissolved in buffer solutions of the same pH, but with an increasing concentration of the buffer. The extent of ionization will increase with increasing buffer concentration owing to reaction of excited 2-naphthol with the weak base form of the buffer.

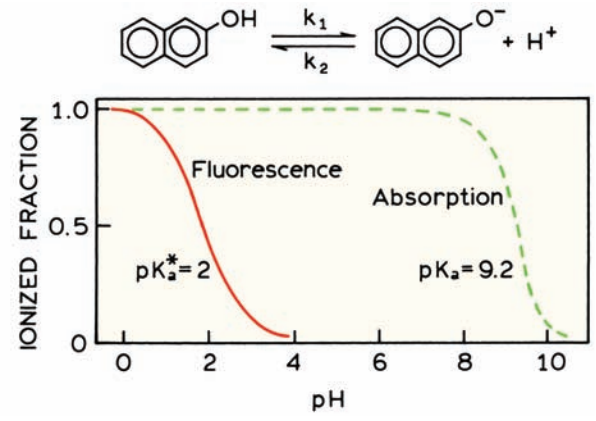

Figure 7.43. Comparison of ground state (dashed) and excited-state (solid) ionization of 2-naphthol.

The spectral shifts that occur upon dissociation in the excited state can be used to calculate the change in pK_A that occurs upon excitation. This is known as the Förster cycle[132–135] (Figure 7.44). The energies of the ground and excited states depend on ionization. Because the dissociation constants are small, the dissociated form of the fluorophore is shown at higher energy. If the pK_A value is lower in the excited state ($pK_A^* < pK_A$), then there is a smaller increase in energy upon dissociation of the excited state ($\Delta H^* < \Delta H$). If one assumes that the entropy change for dissociation is the same for the ground and excited states, then the difference in energy between the ground and excited states of AH and A^- can be related to the change in pK_A values by

$$\Delta pK_A = pK_A - pK_A^* = \frac{E_{HA} - E_{A^-}}{2.3RT} \qquad (7.17)$$

where R is the gas constant and T is the temperature (°K). The energies of the protonated form (E_{HA}) and of the dissociated form (E_A^-) are usually estimated from the average of the absorption $\bar{\nu}_A$ and emission $\bar{\nu}_F$ maxima of each species:

$$E_i = Nhc\frac{\bar{\nu}_A + \bar{\nu}_F}{2} \qquad (7.18)$$

where $\bar{\nu}_A$ and $\bar{\nu}_F$ are in cm^{-1}, h is the Planck constant, N is Avogadro's number, and c is the speed of light.

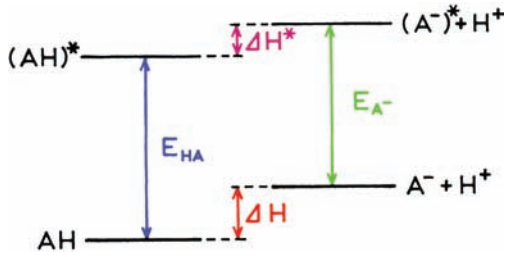

Figure 7.44. Electronic energy levels of an acid AH and its conjugate base A^- in the ground and excited states (the Förster cycle). Reprinted with permission from [131], the *Journal of Chemical Education*, Vol. 69, No. 3, 1992, pp. 247–249. Copyright © 1992, Division of Chemical Education Inc.

While the Förster cycle calculation is useful for understanding the excited-state ionization of fluorophores, the calculated values of ΔpK_A should be used with caution. This is because at 300 nm an error of 4 nm corresponds to a shift of one pK_A unit. Hence the Förster cycle is useful for determining the direction of the change in pK_A but is less reliable in estimating the precise value of pK_A*.

7.12. THEORY FOR A REVERSIBLE TWO-STATE REACTION

The features of an excited-state reaction are illustrated by the Jablonski diagram for the reversible two-state model (Figure 7.45). The terms and subscripts F and R refer to the initially excited and the reacted states, respectively. The decay rates of these species are given by $\gamma_F = \Gamma_F + k_1 + k_{nr}^F$ and $\gamma_R = \Gamma_R + k_2 + k_{nr}^R$, where Γ_F and Γ_R are the radiative decay rates, and k_{nr}^R are the rates of non-radiative decay. The rate of the forward reaction is given by k_1 and the rate of the reverse reaction by k_2. For simplicity we have not included the rates of intersystem crossing to the triplet state, nor the rates of solvent relaxation. Depending upon the specific process under consideration, k_1 and k_2 can each be more complex than a simple rate constant. For example, in the case of a reversible loss of a proton, the reverse rate would be $k_2 = k_2'[H^+]$. In the case of exciplex formation the forward rate would include the concentration of the species (Q) forming the exciplex: $k_1 = k_1'[Q]$. If the reaction is irreversible, $k_2 = 0$. It is simpler to interpret the decay kinetics for irreversible reactions than for reversible reactions. Because there are only two states with well-defined rate constants, it is practical to derive analytical expressions for the steady-state and time-resolved behavior.

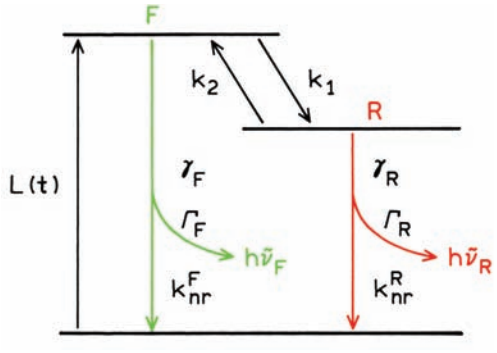

Figure 7.45. Jablonski diagram for a reversible excited-state reaction. $L(t)$ is the excitation function, which can be a pulsed or amplitude-modulated light beam.

7.12.1. Steady-State Fluorescence of a Two-State Reaction

Prior to discussing the time-resolved properties of an excited-state reaction, it useful to describe the spectral properties observed using steady-state methods. Assume that unique wavelengths can be selected where emission occurs only from the unreacted (F) or the reacted (R) states, and assume initially that the reaction is irreversible, that is, $k_2 = 0$ (Figure 7.45). The relative quantum yield of the F state is given by the ratio of the emissive rate to the total rate of depopulation of the F state. Thus,

$$F_0 = \Gamma_F/(\Gamma_F + k_{nr}^F) \tag{7.19}$$

$$F = \Gamma_F/(\Gamma_F + k_{nr}^F + k_1) \tag{7.20}$$

where F_0 and F are the fluorescence intensities observed in the absence and presence of the reaction, respectively. Division of eq. 7.20 by 7.21 yields

$$\frac{F}{F_0} = \frac{1}{1 + k_1\tau_{0F}} \tag{7.21}$$

where $\tau_{0F} = \gamma_F^{-1} = (\Gamma_F + k_{nr}^F)^{-1}$ is the lifetime of the F state in the absence of the reaction. Recall that for a bimolecular rate process k_1 would be replaced by $k_1[Q]$, where Q is the species reacting with the fluorophore. Hence, for some circumstances, the initially excited state can be quenched by a Stern-Volmer dependence.

The yield of the reaction product R is the fraction of F molecules that have reacted. This yield is given by

$$\frac{R}{R_0} = 1 - \frac{F}{F_0} = \frac{k_1\tau_{0F}}{1 + k_1\tau_{0F}} \tag{7.22}$$

where R and R_0 are the intensities of the reacted species when the reaction is incomplete and complete, respectively. In the case of excimer formation, R_0 would be observed at high concentrations of the monomer. It is important to note the distinctly different dependence of the F- and R-state intensities on the extent of the reaction. The intensity of the F state is decreased monotonically to zero as the reaction rate becomes greater than the reciprocal lifetime. In contrast, the intensity of the R state is zero when the forward rate constant is much less than the decay rate of the F state: $k_1 < \gamma_F$ or $k_1\tau_{0F} << 1$. The intensity of the R state increases

to a constant value when $k_1\ \tau_{0F} >> 1$. The reason for this limiting behavior is that essentially all the F state is converted to the R state. In practice, the fluorescence of the reacted species may not reach a limiting value, but may rather decrease as the rate of the forward reaction is increased. This can occur because the conditions needed to drive the reaction to completion may result in other interactions that quench the R state.

7.12.2. Time-Resolved Decays for the Two-State Model

The model described in Figure 7.45 is described by the following kinetic equations:

$$-\frac{d[F]}{dt} = \gamma_F[F] - k_2[R] - L(t) \tag{7.23}$$

$$-\frac{d[R]}{dt} = \gamma_R[R] - k_1[F] \tag{7.24}$$

where $[F]$ and $[R]$ are the concentrations of these states and $L(t)$ is the time profile of the excitation. The solution to these kinetic equations has been described previously with the boundary conditions $[F] = [F_0]$ and $[R] = 0$ at $t = 0$.[129–130,136–137] Following δ-pulse excitation the fluorescence decays of the F and R states are given by expressions of the form

$$I_F(t) = \alpha_1 \exp(-\gamma_1 t) + \alpha_2 \exp(-\gamma_2 t) \tag{7.25}$$

$$I_R(t) = \beta_1 \exp(-\gamma_1 t) - \beta_1 \exp(-\gamma_2 t) \tag{7.26}$$

where the α_i, β_1, and τ_i values are moderately complex functions of the various rate constants. The values of $\gamma_1 = \tau_1^{-1}$ and $\gamma_2 = \tau_2^{-1}$ are given by

$$\gamma_1, \gamma_2 = \frac{1}{2}\{(x + y) \mp [(x + y)^2 + 4k_1k_2]^{1/2}\} \tag{7.27}$$

where

$$x = \Gamma_F + k_{nr}^F + k_1 = \gamma_F + k_1 \tag{7.28}$$

$$y = \Gamma_R + k_{nr}^R + k_2 = \gamma_R + k_2 \tag{7.29}$$

The important point from these equations is that both species display the same decay times, and that the decays of both states is a double exponential decay. Hence, the consequence of a reversible excited-state reaction is that the F and R states both display a double-exponential decay, and that the decay times are the same for both species.

Another important characteristic of an excited-state reaction is seen from the pre-exponential factors for the R state. If only the R state is observed, then the pre-exponential factors (β_1) for the two lifetimes are expected to be equal and opposite (eq. 7.26). The negative pre-exponential factor results in a rise in intensity, which is characteristic of excited-state reactions.

For many molecules that display excited-state reactions there is spectral overlap of the F and R states. If one measures the wavelength-dependent intensity decays this will be described by

$$I(\lambda,t) = \alpha_1(\lambda) \exp(-t/\tau_1) + \alpha_2(\lambda) \exp(-t/\tau_2) \tag{7.30}$$

where the same two decay times will be present at all wavelengths. In this case one can perform a global analysis with two wavelength-independent lifetimes. The meaning of the $\alpha_i(\lambda)$ values is complex, and has been described in detail.[130] As the observation wavelength is increased one observes an increasing fraction of the R state. The $\alpha_i(\lambda)$ values thus shift from those characteristic of the F state (eq. 7.25) to those characteristic of the R state (eq. 7.26). On the long-wavelength side of the emission one expects to observe a negative pre-exponential factor, unless the spectral shift is small so that the F and R states overlap at all wavelengths. The values of $\alpha_i(\lambda)$ can be used to calculate decay-associated spectra (DAS), which shows positive and negative amplitudes. The DAS do not correspond to the emission spectra of either of the species. The $I(\lambda,t)$ data can also be used to calculate the species-associated spectra (SAS), which are the spectra of each of the states (Section 7.14.3).

The theory for an excited-state reaction is considerably simplified if the reaction is irreversible ($k_2 = 0$). In this case eq. 7.27 yields $\gamma_1 = \gamma_F + k_1$ and $\gamma_2 = \gamma_R$. Also, one of the pre-exponential factors in eq. 7.25 becomes zero, so that

$$I_F(t) = \alpha_1 \exp(-\gamma_1 t) \tag{7.31}$$

$$I_R(t) = \beta_1 \exp(-\gamma_1 t) - \beta_1 \exp(-\gamma_2 t) \tag{7.32}$$

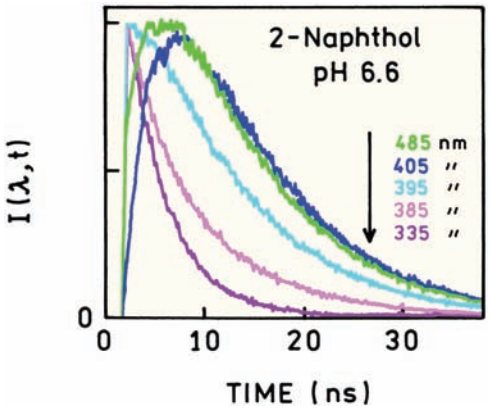

Figure 7.46. Time- and wavelength-dependent intensity decays of 2-naphthol in 10 mM sodium phosphate buffer, pH = 6.6. Revised and reprinted with permission from [141]. Copyright © 2001, American Chemical Society.

Hence, the decay of the initially excited state becomes a single exponential. This prediction has been verified in experimental studies of reversible and irreversible reactions. We note that the negative pre-exponential factor may be associated with either of the decay times (τ_1 or τ_2) depending on the values of the kinetic constants. The negative pre-exponential factor is always associated with the shorter decay time.[138]

7.12.3. Differential Wavelength Methods

In considering excited-state reactions there is a general principle that clarifies the complex decay kinetics and results in simplified methods of analysis.[139–140] This principle is that the population of the *R* state can be regarded as a convolution integral with the *F* state. That is, the F-state population is the excitation pumping function of the *R* state. Consider a measurement of the *R* state, made relative to the *F* state. The *F* state effectively becomes the lamp function, so that measurements relative to the *F* state directly reveal the decay kinetics of the *R* state. The application of this procedure requires a spectral region where the emission from the *F* state can be observed, without overlap from the *R* state. Since non-overlap of states is frequently found on the short-wavelength side of the emission, the time profile of the *F* state can generally be measured directly. Deconvolving the R-state emission with the F-state emission yields the lifetime of the *R* state that would be observed if the *R* state could be directly excited.

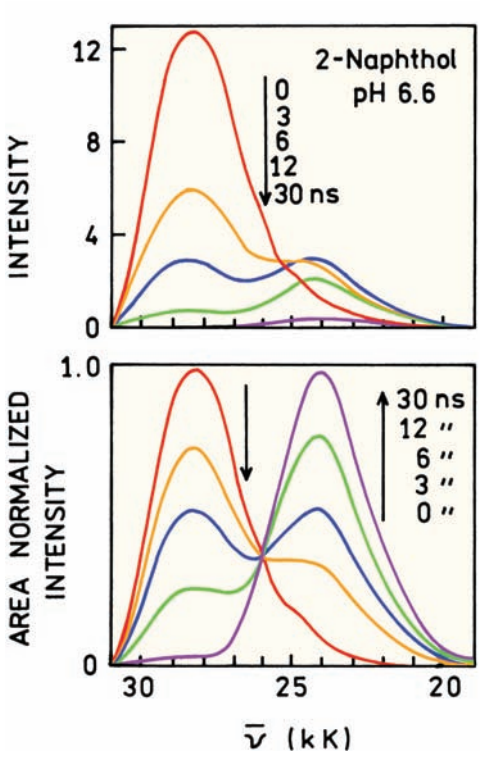

Figure 7.47. Time-resolved emission spectra of 2-naphthol in 10 mM sodium phosphate, pH 6.6. The top panel shows the actual time-resolved intensities. The lower panel shows the area-normalized intensities. Revised and reprinted with permission from [1041. Copyright © 2001, American Chemical Society.

7.13. TIME-DOMAIN STUDIES OF NAPHTHOL DISSOCIATION

The properties of excited-state reactions can be effectively studied using time-domain methods. Typical data for the excited-state ionization of 2-naphthol are shown in Figure 7.46. The time-dependent data were collected at wavelengths across the emission spectrum ranging from 335 to 485 nm.[141] Examination of Figure 7.41 shows the emission at 335 nm is from the unionized form of 2-naphthol and the emission at 485 nm is due to the ionized naphtholate form. The naphtholate emission starts at zero and shows a rise time during which the ionized species is formed.

Time-resolved data collected across the emission spectra can be used to calculate the time-resolved emission spectra (Figure 7.47). The top panel shows the actual time-resolved intensities, not the peak or area-normalized values. As time proceeds the emission from both species decays to zero. At $\tau = 0$ the emission is dominantly due to unionized

2-naphthol. The ionized form shows a transient increase in intensity at time from 3 to 12 ns. These TRES show two distinct emission spectra, which is different from the gradual spectral shifts seen for solvent relaxation. The lower panel in Figure 7.47 shows the TRES that are normalized to the same total area. These spectra show an isoemissive point at 389 nm. Observation of an isoemissive point in the area-normalized TRES proves that there are only two emitting species.[139] An isoemissive point is not expected for continuous spectral relaxation or if there are more than two emitting species.

7.14. ANALYSIS OF EXCITED-STATE REACTIONS BY PHASE-MODULATION FLUOROMETRY

Frequency-domain fluorometry provides a number of interesting opportunities for the analysis of excited-state reactions. One measures the frequency responses across the emission spectra. These data can be used to construct the TRES. However, the data can also be analyzed in terms of the kinetic constants, which leads to insights into the meaning of the measured phase and modulation values. Additional detail can be found elsewhere.[142–144]

For simplicity we consider the irreversible reaction ($k_2 = 0$). Assume that by appropriate optical filtering the emission from the F and R states can be individually observed. Then, relative to the phase and modulation of the excitation, the phase and modulation of the F and R state are given by

$$\tan \phi_F = \omega/(\gamma_F + k_1) = \omega\tau_F \tag{7.33}$$

$$m_F = \frac{\gamma_F + k_1}{\sqrt{(\gamma_F + k_1)^2 + \omega^2}} = \frac{1}{\sqrt{1 + \omega^2\tau_F^2}} \tag{7.34}$$

Several aspects of these equations are worthy of mention. Since we have initially assumed that F and R are separately observable, and the reverse reaction does not occur, the decay of F is a single exponential. Hence, for the F state we find the usual expressions for calculation of lifetimes from phase and modulation data. In the absence of any reaction ($k_1 = 0$) the lifetime is $\tau_{0F} = \gamma_F^{-1}$. In the presence of a reaction, the lifetime of F is shortened to $\tau_F = (\gamma_F + k_1)^{-1}$. Thus, for an irreversible reaction, the observed values of ϕ_F and m_F can be used to calculate the true lifetime of the unreacted state.

The phase and modulation of the R state, when measured relative to the excitation, are complex functions of the various kinetics constants. These values are given by

$$\tan \phi_R = \frac{\omega(\gamma_F + \gamma_R + k_1)}{\gamma_R(\gamma_F + k_1) - \omega^2} \tag{7.35}$$

$$m_R = m_F \frac{\gamma_R}{\sqrt{\gamma_R^2 + \omega^2}} = m_F m_{0R} \tag{7.36}$$

In contrast to the F state, the measured values for the R state cannot be directly used to calculate the R state fluorescence lifetime. The complexity of the measured values (ϕ_R and m_R) shows why it is not advisable to use the apparent phase (τ^ϕ) and modulation (τ^m) lifetimes of the relaxed state.

Closer examination of eqs. 7.33–7.36 reveals important relationships between the phase and modulation values of the F and R states. For an excited-state process, the phase angles of the F and R states are additive, and the modulations multiply. Once this is understood, the complex expressions (eqs. 7.35–7.36) become easier to understand. Let ϕ_{0R} be the phase angle of the R state that would be observed if this state could be excited directly. Of course, this is related to the lifetime of the directly excited R state by $\tan \phi_{0R} = \omega\tau_{0R}$. Using eq. 7.36, the law for the tangent of a sum, and $\tan (\phi_F + \phi_{0R}) = \tan \phi_R$, one finds

$$\phi_R = \phi_F + \phi_{0R} \tag{7.37}$$

Hence, the phase angle of the reacted state, measured relative to the excitation, is the sum of the phase angle of the unreacted state (ϕ_F) and the phase angle of the reacted state, if this state could be directly excited (ϕ_{0R}). This relationship (Figure 7.48) may be understood intuitively by recognizing that the F state is populating the R state. Of course, these are the same considerations used to describe differential-wavelength deconvolution. For the irreversible reaction, measurement of $\Delta\phi = \phi_R - \phi_F = \phi_{0R}$ reveals directly the intrinsic lifetime of the reacted fluorophore, unaffected by its population through the F state.

The demodulation factors of the two states display similar properties. From eq. 7.36 one finds that the demodulation of the relaxed state (m_R) is the product of the demodulation of the unrelaxed state (m_F) and that demodulation due to the intrinsic decay of the R state alone (m_{0R}). That is,

$$m_R = m_F \frac{1}{\sqrt{1 + \omega^2\tau_R^2}} = m_F m_{0R} \tag{7.38}$$

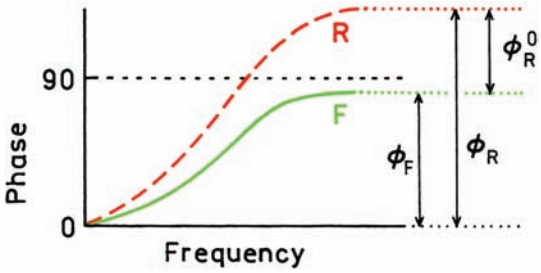

Figure 7.48. Relationship of the phase angles of the *F* and *R* states.

A further interesting aspect of the phase difference or the demodulation between *F* and *R* is the potential of measuring the reverse reaction rate k_2. This reverse rate can be obtained from the phase-angle difference between the *R* and *F* states, or from the modulation of the *R* state relative to the *F* state. For a reversible reaction these expressions are

$$\tan(\phi_R - \phi_F) = \frac{\omega}{(\gamma_R + k_2)} = \omega\tau_R \qquad (7.39)$$

$$\frac{m_R}{m_F} = \frac{\gamma_R + k_2}{\sqrt{(\gamma_R + k_2)^2\omega^2}} = \frac{1}{\sqrt{1 + \omega^2\tau_R^2}} \qquad (7.40)$$

These expressions are similar to the usual expressions for the dependence of phase shift and demodulation on the decay rates of an excited state, except that the decay rate is that of the reacted species ($\gamma_R + k_2$). The initially excited state populates the relaxed state and the reverse reaction repopulates the *F* state. Nonetheless, the kinetic constants of the *F* state do not affect the measurement of tan ($\phi_R - \phi_F$) or m_R/m_F. Measurement of either the phase or modulation of the reacted state, relative to the unrelaxed state, yields a lifetime of the reacted state. This lifetime is decreased by the reverse reaction rate in a manner analogous to the decrease in the lifetime of the *F* state by k_1. If the decay rate (γ_R) is known, k_2 may be calculated. If the emission results from a single species that displays one lifetime, and ϕ and *m* are constant across the emission, then $\phi_R - \phi_F = 0$ and $m_R/m_F = 1$.

Returning to the irreversible model, we note an interesting feature of ϕ_R (eq. 7.35). This phase angle can exceed 90°. Specifically, if ω^2 exceeds γ_R ($\gamma_F + k_1$), then $\tan\phi_R < 0$ or $\phi_R > 90°$. In contrast, the phase angle of directly excited species, or the phase angles resulting from a heterogeneous population of fluorophores, cannot exceed 90°. Therefore, observation of a phase angle in excess of 90° constitutes proof of an excited-state reaction.

7.14.1. Effect of an Excited-State Reaction on the Apparent Phase and Modulation Lifetimes

The multiplicative property of the demodulation factors and the additive property of the individual phase angles are the origin of a reversed frequency dependence of the apparent phase shift and demodulation lifetimes, and the inversion of apparent phase and modulation lifetimes when compared to a heterogeneous sample. The apparent phase lifetime (τ_R^ϕ) calculated from the measured phase (ϕ_R) of the relaxed state is

$$\tan\phi_R = \omega\tau_R^\phi = \tan(\phi_F + \phi_{0R}) \qquad (7.41)$$

Recalling the law for the tangent of a sum one obtains

$$\tau_R^\phi = \frac{\tau_F + \tau_{0R}}{1 - \omega^2\tau_F\tau_{0R}} \qquad (7.42)$$

Because of the term $\omega^2\tau_F\tau_{0R}$, an increase in the modulation frequency can result in an increase in the apparent phase lifetime. This result is opposite to that found for a heterogeneous emitting population where the individual species are excited directly. For a heterogeneous sample an increase in modulation frequency yields a decrease in the apparent phase lifetime.[145] Therefore, the frequency dependence of the apparent phase lifetimes can be used to differentiate a heterogeneous sample from a sample that undergoes an excited-state reactions. Similarly, the apparent modulation lifetime is given by

$$\tau_R^m = \left(\frac{1}{m_R^2} - 1\right)^{-1/2} \qquad (7.43)$$

Recalling eq. 7.36, one obtains

$$\tau_R^m = (\tau_F^2 + \tau_{0R}^2 + \omega^2\tau_F^2\tau_{0R}^2)^{1/2} \qquad (7.44)$$

Again, increasing ω yields an increased apparent modulation lifetime. This frequency dependence is also opposite to that expected from a heterogeneous sample, and is useful in proving that emission results from an excited-state process. In practice, however, the dependence of τ_R^m upon modulation frequency is less dramatic than that of τ_R^ϕ. We again stress that the calculated lifetimes are apparent values and not true lifetimes.

The information derived from phase-modulation fluorometry is best presented in terms of the observed quantities

ϕ and m. For a single-exponential decay, and for the unrelaxed state if relaxation is irreversible, $m_F = \cos \phi_F$. Also $m_{0R} = \cos \phi_{0R}$, irrespective of the reversibility of the reaction. A convenient indicator of an excited-state process is the ratio m/cos ϕ, where m and ϕ are the experimentally measured demodulation factor and phase angle, respectively. This ratio is unity for a single-exponential decay, and is less than one for a heterogeneous emission. In contrast, m/cos $\phi > 1$ if the emitting species forms subsequent to excitation.[146] Using eqs. 7.37 and 7.38, and the law for the cosine of a sum, we obtain

$$\frac{m_R}{\cos \phi_R} = \frac{\cos \phi_{0R} \cos \phi_F}{\cos (\phi_{0R} + \phi_F)}$$

$$= \frac{\cos \phi_{0R} \cos \phi_F}{\cos \phi_{0R} \cos \phi_F - \sin \phi_{0R} \sin \phi_F} \qquad (7.45)$$

Dividing numerator and demodulator by $\cos \phi_{OR} \cos \phi_F$ we obtain

$$\frac{m_R}{\cos \phi_R} = \frac{1}{1 - \tan \phi_{0R} \tan \phi_F} = \frac{1}{1 - \omega^2 \tau_{0R} \tau_F} \qquad (7.46)$$

If relaxation is much slower than emission, significant relaxation does not occur. The R state cannot be observed and eq. 7.46 cannot be applied. If relaxation is much faster than emission, $\phi_F = 0$ and $m_R/\cos \phi_R = 1$. Importantly, if relaxation and emission occur on comparable timescales, ratio $m_R/\cos \phi_R$ exceeds unity. Observation of m/cos $\phi > 1$ proves the occurrence of an excited-state reaction. However, failure to observe m/cos $\phi > 1$ does not prove a reaction has not occurred. Heterogeneity, spectral overlap or the reverse reaction can prevent observation of m/cos $\phi > 1$.

7.14.2. Wavelength-Dependent Phase and Modulation Values for an Excited-State Reaction

The general features of phase-shift and demodulation data for a sample that undergoes an irreversible excited-state reaction is illustrated by the excited-state protonation of acridine by ammonium ion.[143] In basic solution an emission maximum of 430 nm is observed (Figure 7.49). Upon acidification this spectrum is replaced by a red-shifted spectrum with an emission maximum of 475 nm. The former spectrum is due to neutral acridine (Ac) and the latter is due to the acridinium cation (AcH^+). Since the ground-state pK_A of acridine is 5.45, only the neutral species is present at pH = 8.3. Nonetheless, increasing concentrations of ammonium ion, at pH = 8.3, yield a progressive quenching of the short-wavelength emission, with a concomitant appearance of the emission from the acridinium ion (Figure 7.49). These spectral shifts are the result of protonation of the excited neutral acridine molecules by ammonium ions. In the excited state the pK_A of neutral acridine increases from the ground state value of 5.45 to 10.7.

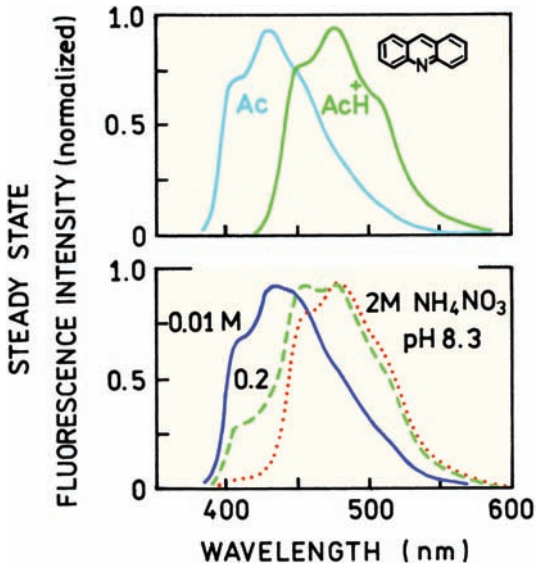

Figure 7.49. Fluorescence emission spectra of acridine. Spectra are shown for the neutral and protonated forms of acridine (top) and of acridine at pH 8.3 with various concentrations of ammonium ion (bottom). Reprinted from [143]. Copyright © 1982, with permission from Elsevier Science.

This excited-state reaction illustrates the phase-modulation theory just described. It is a two-state process that is essentially irreversible. Time-resolved studies demonstrated that at 410 nm the decay is a single exponential.[124] At 560 nm the fluorescence decay can be described with two lifetimes, one of which has the same as the decay time observed at 410 nm. The two lifetimes were independent of emission wavelength, but the pre-exponential factors were dependent on emission wavelength. These data imply that the lifetime of each species (Ac and AcH^+) is constant across its emission spectrum, and that the irreversible two-state theory is appropriate to describe this excited-state process. Examination of the emission spectra (Figure 7.49) reveals a region where only the neutral species emits

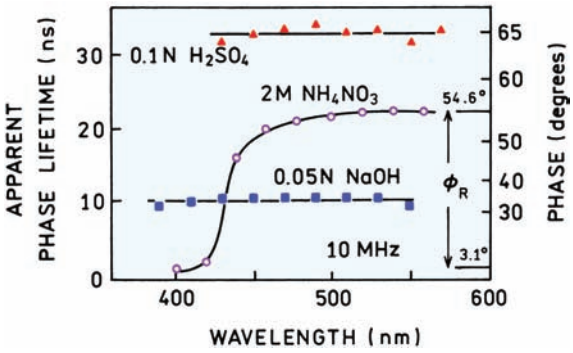

Figure 7.50. Apparent phase lifetimes of acridine. The inserted axis on the right-hand side indicates the phase angles relative to the exciting light. The phase angle difference between the red (ϕ_R = 54.6°) and blue (ϕ_F = 3.1°) regions of the emission reveals the lifetime of the acridinium cation that would be observed if this species could be directly excited. The phase angles of acridinium, relative to the exciting light, do not yield true lifetimes for the directly excited acridinium cation. Reprinted from [143]. Copyright © 1982, with permission from Elsevier Science.

(390–410 nm), a region of strong overlap (440–500 nm), and a region of moderate overlap where the spectrum is dominated by the AcH^+ emission (>500 nm).

The apparent phase lifetimes (τ^ϕ) for acridine in 0.05 N NaOH, 0.1 N H_2SO_4, and 2 M NH_4NO_3 are shown in Figure 7.50. In acidic or basic solution, one species is present in both the ground and excited states, and the lifetimes (or phase angles) are independent of emission wavelength. In contrast, the lifetimes in 2 M NH_4NO_3 are highly dependent upon wavelength because of protonation of acridine subsequent to excitation. At short wavelengths (410 nm), where neutral acridine emits, the lifetime is decreased in the presence of ammonium ion. A decreased phase angle (or lifetime) of the initially excited state is a characteristic feature of an excited-state reaction. At longer wavelengths the apparent lifetime increases until a nearly constant value is reached for wavelengths longer than 500 nm. In this wavelength range the emission is dominated by the acridinium ion. The constant lifetime, or more correctly phase angle, on the red and blue sides of the emission may be regarded as evidence for the two-state model. If the overall emission were shifting to longer wavelengths according to the continuous Bakhshiev model,[1] such regions of constant phase angle are not expected. Overall, the phase data for acridine may be regarded as typical for a two-state reaction with moderate spectral overlap. These characteristics include a decrease in lifetime on the blue side of the emission, an increase in apparent lifetime with emission wavelength, and nearly constant lifetimes on the blue and red sides of the emission.

An interesting potential of phase fluorometry is the ability to measure directly the intrinsic lifetime of the reacted species. By "intrinsic" we mean the lifetime that would be observed if this species were formed by direct excitation, rather than by an excited-state reaction. The intrinsic lifetime of the reacted species is revealed by the phase difference ($\Delta\phi$) between the blue and red sides of the emission ($\Delta\phi = \phi_R - \phi_F$). Consider the phase difference between 400 and 560 nm shown in Figure 7.50. This phase angle difference ($\Delta\phi$ = 51.5°) yields the lifetime of the acridine cation ($\tau(AcH^+)$) according to

$$\tan\Delta\phi = \omega\tau(AcH^+) \tag{7.47}$$

which is found to be 20 ns in 2 M NH_4NO_3. Recall that the origin of this simple result is that the excited neutral acridine population is the pumping function for the excited-state acridinium molecules.

Phase measurements alone, at a single modulation frequency, cannot be used to distinguish between ground-state heterogeneity and an excited-state reaction. The increase in phase angle shown in Figure 7.50 could also be attributed to a second directly excited fluorophore with a longer lifetime. Of course, the decrease in the phase lifetime at short wavelengths indicates a quenching process. A rigorous proof of the presence of an excited-state process is obtainable by comparison of the phase shift and demodulation data from the same sample. Figure 7.51 shows apparent phase and modulation lifetimes and the ratio m/cos ϕ for acridine in 0.2 M NH_4NO_3. On the blue edge $\tau^\phi \simeq \tau^m$ and m/cos $\phi \simeq$

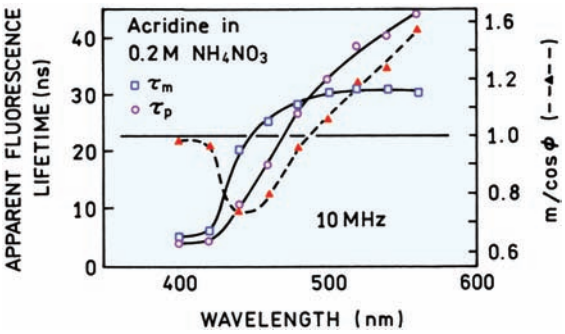

Figure 7.51. Apparent phase (open circle) and modulation (open square) lifetimes of acridine at pH 8.3, 0.2 M NH_4NO_3. Also shown is the wavelength dependence of *m*/cos ϕ (triangle). Reprinted from [143]. Copyright © 1982, with permission from Elsevier Science.

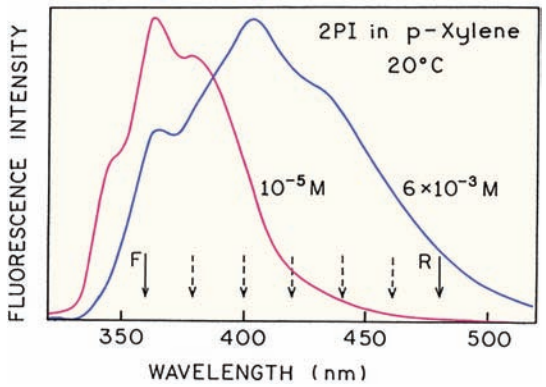

Figure 7.52. Emission spectra of 2-phenylindole in p-xylene at 10^{-5} and 6 x 10^{-3} M. The emission at long wavelengths is due to excimer formation. From [147].

1, indicative of a single-exponential decay and therefore an irreversible reaction. In the central overlap region, $\tau^{\phi} < \tau^{m}$ and m/cos $\phi < 1$, which is indicative of emission from more than one state. At longer wavelengths, $\tau^{\phi} > \tau^{m}$ and *m*/cos $\phi > 1$. These last results are impossible for a multi-exponential decay with any degree of heterogeneity. This observation proves that the emission at these longer wavelengths was not a result of direct excitation, but rather is the result of an excited-state reaction.

7.14.3. Frequency-Domain Measurement of Excimer Formation

In the preceding section we described how the phase and modulation values, when measured at a single modulation frequency, were affected by an excited-state reaction. When using a variable-frequency instrument, the intensity decay can be recovered without a detailed interpretation of the individual phase and modulation values. This is illustrated for excimer formation by 2-phenylindole (2-PI).[147] At higher concentrations of 2-PI there is increased intensity on the long-wavelength sides of the emission (Figure 7.52), which is thought to be due to formation of excimers. However, the long-wavelength emission could also be the result of ground state complexes of 2-PI. These possibilities were distinguished by measurement of the frequency response at various emission wavelengths (arrows in Figure 7.52). The data for observation at 360 nm (*F*) and 480 nm (*R*) are shown in Figure 7.53. At 360 nm (●) a typical frequency response was observed. At 480 nm (○) the phase angles increase rapidly with frequency and exceed 90°, which proves the emission at 480 nm is not directly excited.

The frequency responses at each wavelength were used to recover the intensity decays (Table 7.5). It was possible to fit the data globally with two wavelength-independent lifetimes. As the observation wavelength increases, the amplitude of the 0.86-ns component becomes negative. At 480 nm the amplitudes are nearly equal and opposite, suggesting that there is minimal contribution of the *F* state at this wavelength. If desired, the decay times and amplitudes in Table 7.5 can be used to construct the time-resolved emission spectra (TRES), or the decay-associated spectra (DAS). The decay-associated spectra of the shorter-lifetime component show regions of positive and negative amplitudes (Figure 7.54). This occurs because there is a negative pre-exponential factor associated with this decay time at longer wavelengths.

Another type of calculated spectra are the species-associated spectra (SAS).[148–150] The species-associated spectra are the emission spectra of the individual species if these could be observed individually. The difference between

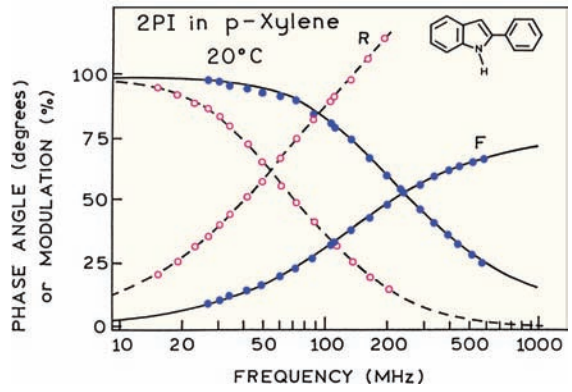

Figure 7.53. Frequency-domain intensity decays of 2-phenylindole (6 x 10^{-3} M) observed at 360 (*F*) and 480 nm (*R*). From [147].

Table 7.5. Wavelength-Dependent Intensity Decays of 2-Phenylindole (6 x 10^{-3} M) in p-Xylene at 20°C

	τ_1 = 0.86 ns[a]		τ_2 = 3.42 ns	
λ_{em} (nm)	α_1	f_1	α_2	f_2
360	0.967	0.879	0.033	0.121
380	0.951	0.831	0.049	0.069
400	0.731	0.405	0.269	0.595
420	–0.047	–0.012	0.953	0.988
440	–0.326	–0.108	0.674	0.892
460	–0.407	–0.147	0.593	0.853
480	–0.453	–0.172	0.547	0.828

[a]The intensity decays measured for each emission wavelength (λ_{em}) were fit with τ_1 and τ_2 as a global parameters. The χ_R^2 of this global fit is 3.9. From [147].

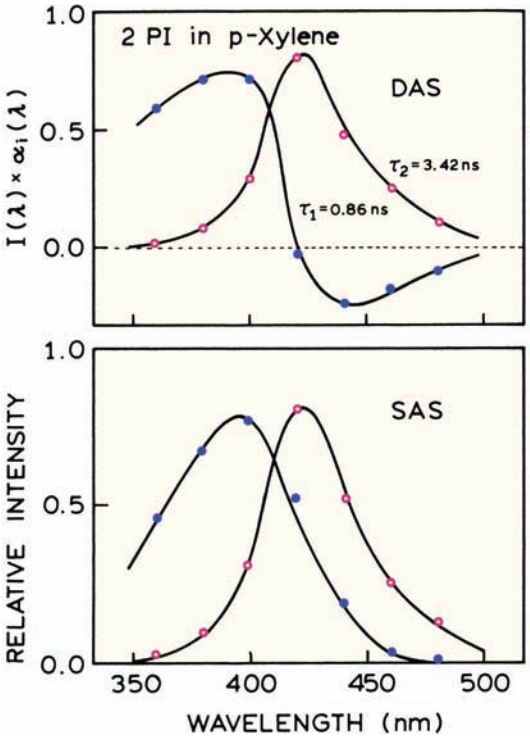

Figure 7.54. Decay-associated spectra (DAS, top) and species-associated spectra (SAS, bottom) for 2 PI (6 x 10^{-3} M) in p-xylene. From [147].

DAS and SAS can be confusing. For ground-state heterogeneity or a mixture of fluorophores, the DAS and SAS are the same because each lifetime is associated with a separate fluorophore. For an excited-state reaction the SAS are more complex. Recall from Section 7.12.2 that for a reversible excited-state reaction both the decays of the *F* and *R* states are both double exponentials. Hence, the DAS are not the emission spectra of each species, but contain contributions from both the *F* and *R* states. The SAS are the emission spectra of the *F* and *R* states, not of a lifetime component. The theory describing the relationship between DAS and SAS is moderately complex and best explained in the papers on this topic.[148–150] For the case of 2-PI, the SAS indicate that the monomer emission of 2-PI is centered near 390 nm, and the excimer emission is only moderately red shifted to 420 nm (Figure 7.54).

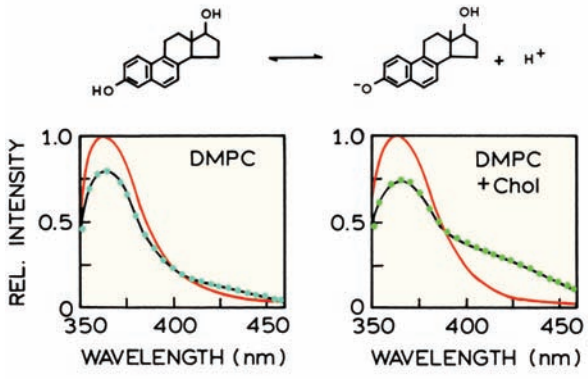

Figure 7.55. **Top**: Excited-state ionization of dihydroequilenin (DHE). **Bottom**: Emission spectra of DHE bound to DMPC vesicles (left) or DMPC vesicles containing 10 mole% cholesterol. Revised and reprinted with permission from [138]. Copyright © 1986, American Chemical Society.

7.15. BIOCHEMICAL EXAMPLES OF EXCITED-STATE REACTIONS

7.15.1. Exposure of a Membrane-Bound Cholesterol Analogue

Excited-state reactions have been used to determine the water accessibility of fluorophores when bound to biomolecules. This is illustrated by the examples of the cholesterol analogue dihydroequilenin (DHE), which can lose a proton in the excited state (Figure 7.55). The emission spectra of DHE were examined when bound to DMPC vesicles without or with 10 mole% cholesterol.[138] The long-wavelength emission from the ionized DHE was more intense in the vesicles which also contained cholesterol. This result indicates that cholesterol displaces DHE towards the surface of the bilayers, allowing deprotonation and thus results in a more intense long-wavelength emission. The concept of an excited-state reaction was also used to study diffusion of lipids in membranes. Similarly, pyrene-labeled lipids were used to determine the extent to which excimer emission was formed by diffusion, or due to preexisting ground state complexes.[151–152] Excimer formation has also been used to study end-to-end motions in polymers.[153–155]

Additional information is available in detailed reports that describe methods to determine the kinetics parameters.[155–161]

REFERENCES

1. Bakhshiev NG, Mazurenko YuT, Piterskaya IV. 1966. Luminescence decay in different portions of the luminescence spectrum of molecules in viscous solution. *Opt Spectrosc* **21**:307–309.
2. Mazurenko YuT, Bakshiev NK. 1970. Effect of orientation dipole relaxation on spectral, time, and polarization characteristics of the luminescence of solutions. *Opt Spectrosc* **28**:490–494.

3. Bakhshiev NK, Mazurenko YuT, Piterskaya IV. 1969. Relaxation effects in the luminescence characteristics of viscous solutions. *Akad Nauk SSSR Bull Phys Sci* **32**:1262–1266.
4. Ware WR, Lee SK, Brant GJ, Chow PP. 1970. Nanosecond time-resolved emission spectroscopy: spectral shifts due to solvent-excited solute relaxation. *J Chem Phys* **54**:4729–4737.
5. Ware WR, Chow P, Lee SK. 1968. Time-resolved nanosecond emission spectroscopy: spectral shifts due to solvent-solute relaxation. *Chem Phys Lett* **2**(6):356–358.
6. Chakrabarti SK, Ware WR. 1971. Nanosecond time-resolved emission spectroscopy of 1-anilino-8-naphthalene sulfonate. *J Chem Phys* **55**(12):5494–5498.
7. Easter JH, DeToma RP, Brand L. 1976. Nanosecond time-resolved emission spectroscopy of a fluorescence probe adsorbed to L-α-egg lecithin vesicles. *Biophys J* **16**:571–583.
8. O'Connor DV, Phillips D. 1984. *Time-correlated single photon counting*, pp. 211–251. Academic Press, New York.
9. Badea MG, Brand L. 1979. Time-resolved fluorescence measurements. *Methods Enzymol* **61**:378–425.
10. Badea MG, De Toma RP, Brand L. 1978. Nanosecond relaxation processes in liposomes. *Biophys J* **24**:197–212.
11. Buzády A, Erostyák J, Somogyi B. 2001. Phase-fluorometry study on dielectric relaxation of acrylodan-labeled human serum albumin. *Biophys Chem* **94**:75–85.
12. Mandal D, Sen S, Sukul D, Bhattacharyya K, Mandal AK, Banerjee R, Roy S. 2002. Solvation dynamics of a probe covalently bound to a protein and in an AOT microemulsion: 4(N-bromoacetylamino)-phthalimide. *J Phys Chem B* **106**:10741–10747.
13. Halder A, Sen P, Das Burman A, Bhattacharyya K. 2004. Solvation dynamics of DCM in a polypeptide-surfactant aggregate: gelatin-sodium dodecyl sulfate. *Langmuir* **20**:653–657.
14. Gafni A, De Toma RP, Manrow RE, Brand L. 1977. Nanosecond decay studies of a fluorescence probe bound to apomyoglobin. *Biophys J* **17**:155–168.
15. Lakowicz JR, Cherek H. 1981. Proof of nanosecond timescale relaxation in apomyoglobin by phase fluorometry. *Biochem Biophys Res Commun* **99**:1173–1178.
16. Lakowicz JR, Gratton E, Cherek H, Maliwal BP, Laczko G. 1984. Determination of time-resolved fluorescence emission spectra and anisotropies of a fluorophore-protein complex using frequency-domain phase-modulation fluorometry. *J Biol Chem* **259**(17): 10967–10972.
17. Pierce DW, Boxer SG. 1992. Dielectric relaxation in a protein matrix. *J Phys Chem* **96**:5560–5566.
18. Wang R, Sun S, Bekos EJ, Bright FV. 1995. Dynamics surrounding Cys-34 in native, chemically denatured, and silica-adsorbed bovine serum albumin. *Anal Chem* **67**:149–159.
19. Demchenko AP, Apell H-J, Stürmer W, Feddersen B. 1993. Fluorescence spectroscopic studies on equilibrium dipole-relaxational dynamics of Na,K-ATPase. *Biophys Chem* **48**:135–147.
20. Pal SK, Mandal D, Sukul D, Sen S, Bhattacharyya K. 2001. Solvation dynamics of DCM in human serum albumin. *J Phys Chem B* **105**:1438–1441.
21. Sen P, Mukherjee S, Dutta P, Halder A, Mandal D, Banerjee R, Roy S, Bhattachyaryya K. 2003. Solvation dynamics in the molten glouble state of a protein. *J Phys Chem B* **107**:14563–14568.
22. Hutterer R, Hof M. 2001. Dynamics in diether lipid bilayers and interdigitated bilayer structures studied by time-resolved emission spectra, decay time and anisotropy profiles. *J Fluoresc* **11**(3):227–236.
23. Hutterer R, Hof M. 2002. Probing ethanol-induced phospholipid phase transitions by the polarity sensitive fluorescence probes prodan and patman. *Z Phys Chem* **216**:333–346.
24. Easter JH, Detoma RP, Brand L. 1978. Fluorescence measurements of environmental relaxation at the lipid–water interface region of bilayer membranes. *Biochem Biophys Acta* **508**:27–38.
25. DeToma RP, Easter JH, Brand L. 1976. Dynamic interactions of fluorescence probes with the solvent environment. *J Am Chem Soc* **98**: 5001–5007.
26. Lakowicz JR, Cherek H, Laczko G, Gratton E. 1984. Time-resolved fluorescence emission spectra of labeled phospholipid vesicles, as observed using multi-frequency phase-modulation fluorometry. *Biochim Biophys Acta* **777**:183–193.
27. Parasassi T, Conti F, Gratton E. 1986. Time-resolved fluorescence emission spectra of laurdan in phospholipid vesicles by multifrequency phase and modulation fluorometry. *Cell Mol Biol* **32**(1):103–108.
28. Sommer A, Paltauf F, Hermetter A. 1990. Dipolar solvent relaxation on a nanosecond timescale in ether phospholipid membranes as determined by multifrequency phase and modulation fluorometry. *Biochemistry* **29**:11134–11140.
29. Hutterer R, Schneider FW, Lanig H, Hof M. 1997. Solvent relaxation behaviour of n-anthroyloxy fatty acids in PC-vesicles and paraffin oil: a time-resolved emission spectra study. *Biochim Biophys Acta* **1323**:195–207.
30. Hof M, Hutterer R. 1998. Solvent relaxation of fluorescent labels as a new tool for the detection of polarity and rigidity changes in membranes. *Czech J Phys* **48**(4):435–441.
31. Sykora J, Mudogo V, Hutterer R, Nepras M, Vanerka J, Kapusta P, Fidler V, Hof M. 2002. ABA-C_{15}: a new dye for probing solvent relaxation in phospholipid bilayers. *Langmuir* **18**:9276–9282.
32. Pal SK, Sukul D, Mandal D, Bhattacharyya K. 2000. Solvation dynamics of DCM in lipid. *J Phys Chem B* **104**:4529–4531.
33. Dutta P, Sen P, Mukherjee S, Bhattacharyya K. 2003. Solvation dynamics in DMPC vesicle in the presence of a protein. *Chem Phys Lett* **382**:426–433.
34. Chakrabarty D, Hazra P, Chakraborty A, Sarkar N. 2003. Solvation dynamics of coumarin 480 in bile salt–cetyltrimethylammonium bromide (CTAB) and bile salt–tween 80 mixed micells. *J Phys Chem B* **107**:13543–13648.
35. Hara K, Kuwabara H, Kajimoto O. 2001. Pressure effect on solvation dynamics in micellar environment. *J Phys Chem B* **105**:7174–7179.
36. Balasubramanian S, Bagchi B. 2001. Slow solvation dynamics near an aqueous micellar surface. *J Phys Chem B* **105**:12529–12533.
37. Maciejewski A, Kubicki J, Dobek K. 2003. The origin of time-resolved emission spectra (TRES) changes of 4-aminophthalimide (4-AP) in SDS micelles: the role of the hydrogen bond between 4-AP and water present in micelles. *J Phys Chem B* **107**:13986–13999.
38. Corbeil EM, Levinger NE. 2003. Dynamics of polar solvation in quaternary microemulsions. *Langmuir* **19**:7264–7270.
39. Sarkar R, Ghosh M, Pal SK. 2005. Ultrafast relaxation dynamics of a biologically relevant probe dansyl at the micellar surface. *J Photochem Photobiol B* **78**(2):93–98.

40. Egelhaaf H-J, Lehr B, Hof M, Häfner A, Fritz H, Schneider FW, Bayer E, Oelkrug D. 2000. Solvation and solvent relaxation in swellable copolymers as studied by time-resolved fluorescence spectroscopy. *J Fluoresc* **10**(4):383–392.
41. Shirota H, Segawa H. 2003. Time-resolved fluorescence study on liquid oligo(ethylene oxide)s: coumarin 153 in poly(ethylene glycol)s and crown ethers. *J Phys Chem A* **107**:3719–3727.
42. Bhattacharyya K. 2005. Organized assemblies probed by fluorescence spectroscopy. In *Reviews in fluorescence*, pp. 1–19. Ed C Geddes, JR Lakowicz. Springer Verlag, New York.
43. Stryer L. 1965. The interactions of a naphthalene dye with apomyoglobin and apohemoglobin: a fluorescent probe of non-polar binding sites. *J Mol Biol* **13**:482–495.
44. Murakami H, Kushida T. 1994. Fluorescence properties of Zn-substituted myoglobin. *J Luminesc* **58**:172–175.
45. Cohen BE, McAnaney TB, Park ES, Jan YN, Boxer SG, Jan LY. 2002. Probing protein electrostatics with a synthetic fluorescent amino acid. *Science* **296**:1700–1703.
46. Kobayashi N, Honda S, Yoshii H, Munekata E. 2000. Role of side-chains in the cooperative β-hairpin folding of the short c-terminal fragment derived from streptococcal protein G. *Biochemistry* **39**: 6564–6571.
47. Park SH, Shastry MCR, Roder H. 1999. Folding dynamics of the B1 domain of protein G explored by ultrarapid mixing. *Nat Struct Mol Biol*. **6**(10):943–947.
48. Easter JH, Brand L. 1973. Nanosecond time-resolved emission spectroscopy of a fluorescence probe bound to L-α-egg lecithin vesicles. *Biochem Biophys Res Comm* **52**(3):1086–1092.
49. Molotsky T, Huppert D. 2003. Site specific solvation statics and dynamics of coumarin dyes in hexane-methanol mixture. *J Phys Chem A* **107**(16):2769–2780.
50. Pal SK, Zhao L, Zewail AH. 2003. Water at DNA surfaces: ultrafast dynamics in minor groove recognition. *Proc Natl Acad Sci USA* **100**(14):8113–8118.
51. Fleming GR, Cho M. 1996. Chromophore-solvent dynamics. *Annu Rev Phys Chem* **47**:109–134.
52. Simon JD. 1988. Time-resolved studies of solvation in polar media. *Acc Chem Res* **21**:128–134.
53. Chapman CF, Fee RS, Maroncelli M. 1995. Measurements of the solute dependence of solvation dynamics in 1-propanol: the role of specific hydrogen-bonding interactions. *J Phys Chem* **99**:4811–4819.
54. Glasbeek M, Zhang H. 2004. Femtosecond studies of solvation and intramolecular configurational dynamics of fluorophores in liquid solution. *Chem Rev* **104**:1929–1954.
55. Bhattacharyya K. 2003. Solvation dynamics and proton transfer in supramolecular assemblies. *Acc Chem Res* **36**(2):95–101.
56. Bhattacharyya K, Bagchi B. 2000. Slow dynamics of constrained water in complex geometries. *J Phys Chem A* **104**:10603–10613.
57. Smith NA, Meech SR, Rubtsov IV, Yoshihara K. 1999. LDS-750 as a probe of solvation dynamics: a femosecond time-resolved fluorescence study in liquid aniline. *Chem Phys Lett* **303**:209–217.
58. Murakami H. 2000. Femtosecond time-resolved fluorescence spectra of a coumarin dye in glycerol. *J Mol Liq* **89**:33–45.
59. Benderskii AV, Eisenthal KB. 2000. Effect of organic surfactant on femosecond solvation dynamics at the air–water interface. *J Phys Chem B* **104**:11723–11728.
60. Liu J-Y, Fan W-H, Han K-L, Xu D-L, Lou N-Q. 2003. Ultrafast dynamics of dye molecules in solution as a function of temperature. *J Phys Chem A* **107**:1914–1917.
61. Jarzeba W, Walker GC, Johnson AE, Kahlow MA, Barbara PF. 1988. Femtosecond microscopic solvation dynamics of aqueous solutions. *J Phys Chem* **92**:7039–7041.
62. Friedman HL. 1983. Fast response of a dielectric to the motion of a charge. *J Chem Soc Faraday Trans* 79:1465–1467.
63. Bagchi B, Oxtoby DW, Fleming GR. 1984. Theory of the time development of the Stokes shift in polar media. *Chem Phys* **86**:257–267.
64. Castner EW, Fleming GR, Bagchi B. 1988. Influence of non-Debye relaxation and of molecular shape on the time dependence of the Stokes in shift polar media. *Chem Phys Lett* **143**(3):270–276.
65. Castner EW, Bagchi B, Maroncelli M, Webb SP, Ruggiero AJ, Fleming GR. 1988. The dynamics of polar solvation. *Ber Bunsenges Phys Chem* **92**:363–372.
66. Bakhshiev NG. 1964. Universal intermolecular interactions and their effect on the position of the electronic spectra of molecules in two-component solutions, VII: theory (general case of an isotropic solution). *Opt Spectrosc* **16**:446–451.
67. Castner EW, Fleming GR, Bagchi B, Maroncelli M. 1988. The dynamics of polar solvation: inhomogeneous dielectric continuum models. *J Chem Phys* **89**:3519–3534.
68. Piterskaya IV, Bakhshiev NG. 1963. Quantitative investigation of the temperature dependence of the absorption and fluorescence spectra of complex molecules. *Akad Nauk SSSR Bull Phys Ser* **27**:625–629.
69. Bushuk BA, Rubinov AN. 1997. Effect of specific intermolecular interactions on the dynamics of fluorescence spectra of dye solutions. *Opt Spectrosc* **82**(4):530–533.
70. Kaatze U, Uhlendorf V. 1981. The dielectric properties of water at microwave frequencies. *Z Phys Chem Neu Folge* **126**:151–165.
71. Cole KS, Cole RH. 1941. Dispersion and absorption in dielectrics. *J Chem Phys* **9**:341–351.
72. Fellner-Feldegg H. 1969. The measurement of dielectrics in the time domain. *J Phys Chem* **75**:616–623.
73. Davidson DW, Cole RH. 1951. Dielectric relaxation in glycerol, propylene glycol, and n-propanol. *J Chem Phys* **19**(12):1484–1490.
74. Denny DJ, Cole RH. 1955. Dielectric properties of methanol and methanol-1-propanol solutions. *J Chem Phys* **23**(10):1767–1772.
75. McDuffie GE, Litovitz TA. 1962. Dielectric relaxation in associated liquids. *J Chem Phys* **37**(8):1699–1705.
76 Gard SK, Smyth CP. 1965. Microwave absorption and molecular structure in liquids, LXII: the three dielectric dispersion regions of the normal primary alcohols. *J Phys Chem* **69**:1294–1301.
77. Bamford CH, Compton RG. 1985. *Chemical kinetics*. Elsevier, New York.
78. Szmacinski H, Gryczynski I, Lakowicz JR. 1996. Resolution of multi-exponential spectral relaxation of Yt-base by global analysis of collisionally quenched samples. *J Fluoresc* **6**(3):177–185.
79. Castner EW, Maroncelli M, Fleming GR. 1987. Subpicosecond resolution studies of solvation dynamics in polar aprotic and alcohol solvents. *J Chem Phys* **86**(3):1090–1097.
80. Frauchiger L, Shirota H, Uhrich KE, Castner EW. 2002. Dynamic fluorescence probing of the local environments within amphiphilic starlike macromolecules. *J Phys Chem B* **106**:7463–7468.

81. Röcker C, Heilemann A, Fromherz P. 1996. Time-resolved fluorescence of a hemicyanine dye: dynamics of rotamerism and resolvation. *J Phys Chem* **100**:12172–12177.
82. Knutson JR, Walbridge DG, Brand L. 1982. Decay associated fluorescence spectra and the heterogeneous emission of alcohol dehydrogenase. *Biochemistry* **21**:4671–4679.
83. Weber G, Lakowicz JR. 1973. Subnanosecond solvent relaxation studies by oxygen quenching of fluorescence. *Chem Phys Lett* **22**:419–423.
84. Rotkiewicz K, Grabowski ZR, Jasny J. 1975. Picosecond isomerization kinetics of excited p-dimethylaminobenzonitriles studied by oxygen quenching of fluorescence. *Chem Phys Lett* **34**:55–100.
85. Lakowicz JR, Hogen D. 1981. Dynamic properties of the lipid–water interface of model membranes as revealed by lifetime-resolved fluorescence emission spectra. *Biochemistry* **20**:1366–1373.
86. Raghuraman H, Kelkar DA, Chattopadhyay A. 2005. Novel insights into protein structure and dynamics utilizing the red edge excitation shift approach. In *Reviews in fluorescence*, pp. 199–222. Ed C Geddes, JR Lakowicz. Springer Verlag, New York.
87. Demchenko AP. 2002. The red-edge effects: 30 years of exploration. *Luminescence* **19**:19–42.
88. Rawat SS, Chattopadhyay A. 1999. Structural transition in the micellar assembly: a fluorescence study. *J Fluoresc* **9**(3):233–243.
89. Mukherjee S, Chattopadhyay A. 1995. Wavelength-selective fluorescence as a novel tool to study organization and dynamics in complex biological systems. *J Fluoresc* **5**(3):237–246.
90. Rawat SS, Mukherjee S, Chattopadhyay A. 1997. Micellar organization and dynamics: a wavelength-selective fluorescence approach. *J Phys Chem B* **101**:1922–1929.
91. Rudik KI, Pikulik LG. 1971. Effect of the exciting light on the fluorescence spectra on phthalmide solutions. *Opt Spectrosc* **30**: 147–148.
92. Rubinov AN, Tomin VI. 1970. Bathochromic luminescence in solutions of organic dyes at low temperatures. *Opt Spectrosc* **29**: 578–580.
93. Galley WC, Purkey RM. 1970. Role of heterogeneity of the solvation site in electronic spectra in solution. *Proc Natl Acad Sci USA* **67**(3): 1116–1121.
94. Itoh K, Azumi T. 1973. Shift of emission band upon excitation at the long wavelength absorption edge. *Chem Phys Lett* **22**(2):395–399.
95. Azumi T, Itoh K, Shiraishi H. 1976. Shift of emission band upon the excitation at the long wavelength absorption edge, III: temperature dependence of the shift and correlation with the time dependent spectral shift. *J Chem Phys* **65**(7):2550–2555.
96. Itoh K, Azumi T. 1975. Shift of the emission band upon excitation at the long wavelength absorption edge, II: importance of the solute–solvent interaction and the solvent reorientation relaxation process. *J Chem Phys* **62**(9):3431–3438.
97. Kawski A, Ston M, Janic I. 1983. On the intensity distribution within photoluminescence bands in rigid and liquid solutions. *Z Naturforsch A* **38**:322–324.
98. Lakowicz JR, Keating-Nakamoto S. 1984. Red-edge excitation of fluorescence and dynamic properties of proteins and membranes. *Biochemistry* **23**:3013–3021.
99. Demchenko AP. 1982. On the nanosecond mobility in proteins, Edge excitation fluorescence red shift of protein-bound 2-(p-toluidinyl-naphthalene)-6-sulfonate. *Biophys Chem* **15**:101–109.
100. Shcherbatska NV, van Hoek A, Visser AJWG, Koziol J. 1994. Molecular relaxation spectroscopy of lumichrome. *J Photochem Photobiol A: Chem* **78**:241–246.
101. Chattopadhyay A, Mukherjee S. 1993. Fluorophore environments in membrane-bound probes: a red edge excitation shift study. *Biochemistry* **32**:3804–3811.
102. Chattopadhyay A, Mukherjee S. 1999. Red edge excitation shift of a deeply embedded membrane probe: implications in water penetration in the bilayer. *J Phys Chem B* **103**:8180–8185.
103. Demchenko AP, Shcherbatska NV. 1985. Nanosecond dynamics of charged fluorescent probes at the polar interface of a membrane phospholipid bilayer. *Biophys Chem* **22**:131–143.
104. Raudino A, Guerrera F, Asero A, Rizza V. 1983. Application of red-edge effect on the mobility of membrane lipid polar head groups. *FEBS Lett* **159**(1,2):43–46.
105. de Oliveira AHC, Giglio JR, Andrião-Escarso SH, Ward RJ. 2001. The effect of resonance energy homotransfer on the intrinsic tryptophan fluorescence emission of the bothropstoxin-I dimer. *Biochem Biophys Res Commun* **284**:1011–1015.
106. Chattopadhyay A, Rukmini R. 1993. Restricted mobility of the sole tryptophan in membrane-bound melittin. *Fed Eur Biochem Soc* **335**(3):341–344.
107. Ghosh AK, Rukmini R, Chattopadhyay A. 1997. Modulation of tryptophan environment in membrane-bound melittin by negatively charged phospholipids: implications in membrane organization and function. *Biochemistry* **36**:14291–14305.
108. Guha S, Rawat SS, Chattopadhyay A, Bhattacharyya B. 1996. Tubulin conformation and dynamics: a red edge excitation shift study. *Biochemistry* **35**:13426–13433.
109. Demchenko AP, Ladokhin AS. 1988. Temperature-dependent shift of fluorescence spectra without conformational changes in protein: studies of dipole relaxation in the melittin molecule. *Biochim Biophys Acta* **955**:352–360.
110. Weber G, Shinitzky M. 1970. Failure of energy transfer between identical aromatic molecules on excitation at the long wave edge of the absorption spectrum. *Proc Natl Acad Sci USA* **65**(4):823–830.
111. Valeur B, Weber G. 1977. Anisotropic rotations in 1-naphthylamine, existence of a red-edge transition moment normal to the ring plane. *Chem Phys Lett* **45**(1):140–144.
112. Valeur B, Weber G. 1978. A new red-edge effect in aromatic molecules: anomaly of apparent rotation revealed by fluorescence polarization. *J Phys Chem* **69**(6):2393–2400.
113. Mantulin WW, Weber G. 1977. Rotational anisotropy and solvent-fluorophore bonds: an investigation by differential polarized-phase fluorometry. *J Chem Phys* **66**(9):4092–4099.
114. Tolbert LM, Solntsev KM. 2002. Excited-state proton transfer: from constrained systems to "super" photoacids to superfast proton transfer. *Acc Chem Res* **35**:19–27.
115. Yang R, Schulman SG. 2001. Kinetics of excited-state proton transfer of doubly protonated 2-aminoacridine. *J Fluoresc* **11**(2):109–112.
116. Cohen B, Huppert D, Agmon N. 2001. Diffusion-limited acid–base nonexponential dynamics. *J Phys Chem A* **105**:7165–7173.
117. Leiderman P, Genosar L, Koifman N, Huppert D. 2004. Effect of pressure on the proton-transfer rate from a photoacid to a solvent, 2: 2-naphthol-6-sulfonate in water. *J Phys Chem A* **108**:2559–2566.
118. Mironczyk A, Jankowski A, Chyla A, Ozyhar A, Dobryszycki P. 2004. Investigation of excited-state proton transfer in 2-naphthol

derivatives included in Langmuir-Blodgett films. *J Phys Chem A* **108**:5308–5314.
119. Cohen B, Huppert D. 2001. Excited state proton-transfer reactions of coumarin 4 in protic solvents. *J Phys Chem A* **105**:7157–7164.
120. Ameer-Beg S, Ormson SM, Poteau X, Brown RG, Foggi P, Bussotti L, Neuwahl FVR. 2004. Ultrafast measurements of charge and excited-state intramolecular proton transfer in solutions of 4'-(N,N-dimethylamino) derivatives of 3-hydroxyflavone. *J Phys Chem A* **108**:6938–6943.
121. Kleinman MH, Flory JH, Tomalia DA, Turro NJ. 2000. Effect of protonation and PAMAM dendrimer size on the complexation and dynamic mobility of 2-naphthol. *J Phys Chem B* **104**:11472–11479.
122. Ireland JF, Wyatt PAH. 1976. Acid–base properties of electronically excited states of organic molecules. In *Advances in physical organic chemistry*, pp. 132–215. Ed V Gold, D Bethell. Academic Press, New York.
123. Wan P, Shukla D. 1993. Utility of acid–base behavior of excited states of organic molecules. *Chem Rev* **93**:571–584.
124. Gafni A, Brand L. 1978. Excited state proton transfer reactions of acridine studied by nanosecond fluorometry. *Chem Phys Lett* **58**: 346–350.
125. Harris CM, Sellinger BK. 1980. Acid–base properties of 1-naphthol: proton-induced fluorescence quenching. *J Phys Chem* **84**:1366–1371.
126. Mandal D, Pal SK, Bhattacharyya B. 1998. Excited-state proton transfer of 1-naphthol in micelles. *J Phys Chem A* **102**:9710–9714.
127. Boyer R, Deckey G, Marzzacco C, Mulvaney M, Schwab C, Halpern AM. 1985. The photophysical properties of 2-naphthol. *J Chem Educ* **62**:630–632.
128. Bardez E, Monnier E, Valeur B. 1985. Dynamics of excited-state reactions in reversed micelles, 2: proton transfer involving various fluorescent probes according to their sites of solubilization. *J Phys Chem* **89**:5031–5036.
129. Loken MR, Hayes JW, Gohlke JR, Brand L. 1972. Excited-state proton transfer as a biological probe: determination of rate constants by means of nanosecond fluorometry. *Biochemistry* **11**:4779–4786.
130. Laws WR, Brand L. 1979. Analysis of two-state excited-state reactions: the fluorescence decay of 2-naphthol. *J Phys Chem* **83**(7): 795–802.
131. Marciniak B, Kozubek H, Paszyc S. 1992. Estimation of pKa in the first excited single state. *J Chem Educ* **69**(3):247–249.
132. Förster Th. 1950. Die pH-abhangigkeit der fluoreszenz von naphthalinderivaten. *Z Electrochem* **54**:531–553.
133. Grabowski ZR, Grabowska A. 1976. The Förster cycle reconsidered. *Z Phys Chem Neu Folge* **104**:197–208.
134. Grabowski ZR. 1981. Generalized Förster cycle applied to coordination compounds. *J Luminesc* **24/25**:559–562.
135. Grabowski ZR, Rubaszewska W. 1977. Generalised Förster cycle. *J Chem Soc Faraday* **73**:11–28.
136. Birks JB. 1970. *Photophysics of aromatic molecules*, pp. 300–309. Wiley-Interscience, New York.
137. Brand L, Laws WR. 1983. Excited-state proton transfer. In *Time-resolved fluorescence spectroscopy in biochemistry and biology*, pp. 319–340. Ed RD Cundall, FE Dale. Plenum, New York.
138. Davenport L, Knutson JR, Brand L. 1986. Excited-state proton transfer of equilenin and dihydroequilenin: interaction with bilayer vesicles. *Biochemistry* **25**:1186–1195.
139. Lakowicz JR, Balter A. 1982. Differential wavelength deconvolution of time-resolved fluorescence intensities: a new method for the analysis of excited state processes. *Biophys Chem* **16**:223–240.
140. Rumbles G, Smith TA, Brown AJ, Carey M, Soutar I. 1997. Autoreconvolution: an extension to the "reference convolution" procedure for the simultaneous analysis of two fluorescence decays from one sample. *J Fluoresc* **7**(3):217–229.
141. Koti ASR, Krishna MMG, Periasamy N. 2001. Time-resolved area-normalized emission spectroscopy (TRANES): a novel method for confirming emission from two excited states. *J Phys Chem A* **105**:1767–1771.
142. Lakowicz JR, Balter A. 1982. Theory of phase-modulation fluorescence spectroscopy for excited state processes. *Biophys Chem* **16**:99–115.
143. Lakowicz JR, Balter A. 1982. Analysis of excited state processes by phase-modulation fluorescence spectroscopy. *Biophys Chem* **16**:117–132.
144. Lakowicz JR, Balter A. 1982. Detection of the reversibility of an excited state reaction by phase modulation fluorometry. *Chem Phys Lett* **92**(2):117–121.
145 Spencer RD, Weber G. 1969. Measurement of subnanosecond fluorescence lifetimes with a cross-correlation phase fluorometer. *Ann NY Acad Sci* **158**:361–376.
146. Veselova TV, Limareva LA, Cherkasov AS, Shirokov VI. 1965. Fluorometric study of the effect of solvent on the fluorescence spectrum of 3-amino-N-methylphthalimide. *Opt Spectrosc* **19**:39–43.
147. Gryczynski I. Unpublished observations.
148. Löfroth J-E. 1985. Recent developments in the analysis of fluorescence intensity and anisotropy data. In *Analytical instrumentation*, pp. 403-431. Ed JWG Visser. Marcel Dekker, New York.
149. Krishna MMG. 1999. Excited-state kinetics of the hydrophobic probe nile red in membranes and micelles. *J Phys Chem A* **103**(19): 3589–3595.
150. Lofroth JE. 1986. Time-resolved emission spectra, decay-associated spectra, and species-associated spectra. *J Phys Chem* **90**:1160–1168.
151. Hresko RC, Sugar IP, Barenholz Y, Thompson TE. 1986. Lateral distribution of a pyrene-labeled phosphatidylcholine in phosphatidylcholine bilayers: fluorescence phase and modulation study. *Biochemistry* **25**:3813–3823.
152. Novikov EG, Visser JWG. 2001. Inter- and intramolecular dynamics of pyrenyl lipids in bilayer membranes from time-resolved fluorescence spectroscopy. *J Fluoresc* **11**(4):297–305.
153. Farinha JPS, Picarra S, Miesel K, Martinho JMG. 2001. Fluorescence study of the coil-globule transition of a PEO chain in toluene. *J Phys Chem B* **105**:10536–10545.
154. Mathew AK, Siu H, Duhamel J. 1999. A blob model to study chain folding by fluorescence. *Macromolecules* **32**:7100–7108.
155. Boens N, Kowalczyk A. 1996. Identifiability of competitive intermolecular three-state excited-state processes. *Chem Phys Lett* **260**: 326–330.
156. Beechem JM, Ameloot M, Brand L. 1985. Global analysis of fluorescence decay surfaces: excited-state reactions. *Chem Phys Lett* **120**(4,5):466–472.
157. Ameloot M, Boens N, Andriessen R, Van den Bergh V, De Schryver FC. 1991. Non a priori analysis of fluorescence decay surfaces of excited-state processes, 1: theory. *J Phys Chem* **95**:2041–2047.

158. Andriessen R, Boens N, Ameloot M, De Schryver FC. 1991. Non a priori analysis of fluorescence decay surfaces of excited-state processes, 2: intermolecular excimer formation of pyrene. *J Phys Chem* **95**:2047–2058.
159. Boens N, Andriessen R, Ameloot M, Van Dommelen L, De Schryver FC. 1992. Kinetics and identifiability of intramolecular two-state excited state processes: global compartmental analysis of the fluorescence decay surface. *J Phys Chem* **96**:6331–6342.
160. Van Dommelen L, Boens N, Ameloot M, De Schryver FC, Kowalczyk A. 1993. Species-associated spectra and upper and lower bounds on the rate constants of reversible intramolecular two-state excited state processes with added quencher: global compartmental analysis of the fluorescence decay surface. *J Phys Chem* **97**: 11738–11753.
161. Van Dommelen L, Boens N, De Schryver FC, Ameloot M. 1995. Distinction between different competing kinetic models of irreversible intramolecular two-state excited-state processes with added quencher: global compartmental analysis of the fluorescence decay surface. *J Phys Chem* **99**:8959–8971.
162. Brand L, Seliskar CJ, Turner DC. 1971. The effects of chemical environment on fluorescence probes. In *Probes of structure and function of macromolecules and membranes*, pp. 17–39. Ed B Chance, CP Lee, JK Blaisie. Academic Press, New York.
163. Gakamsky DM, Demchenko AP, Nemkovich NA, Rubinov AN, Tomin VI, Shcherbatska NV. 1992. Selective laser spectroscopy of 1-phenylnaphthylamine in phospholipid membranes. *Biophys Chem* **42**:49–61.

PROBLEMS

P7.1. *Estimation of the Spectral Relaxation Time*: Figure 7.56 shows time-dependent intensity decays of TNS bound to egg lecithin vesicles.[162] The wavelengths of 390, 435, and 530 nm are on the blue, center, and red regions of the emission spectrum. Use the data in Figure 7.56 to calculate the spectral relaxation time for the TNS-labeled residue. Assume that the emission at 390 nm is dominated by the initially excited states (F) and that the emission at 435 nm represents the TNS, unaffected by relaxation.

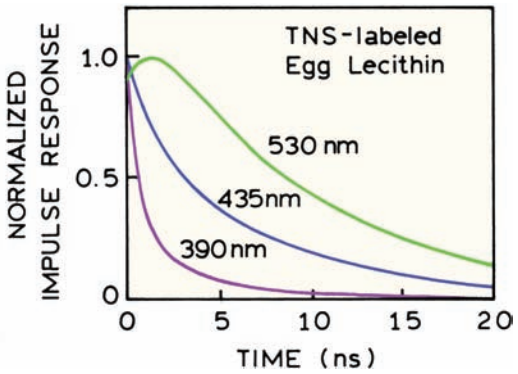

Figure 7.56. Fluorescence impulse response functions of TNS-labeled egg lecithin vesicles. Time-dependent intensities are shown for 390, 435, and 530 nm. From [162].

P7.2. *Interpretation of Wavelength-Dependent Lifetimes*: TNS was dissolved in various solvents or bound to vesicles of dialeoyl-L-α-phosphatidylcholine (DOPC). Apparent phase and modulation lifetimes were measured across the emission spectra of these samples. Explain these data in Figure 7.57.

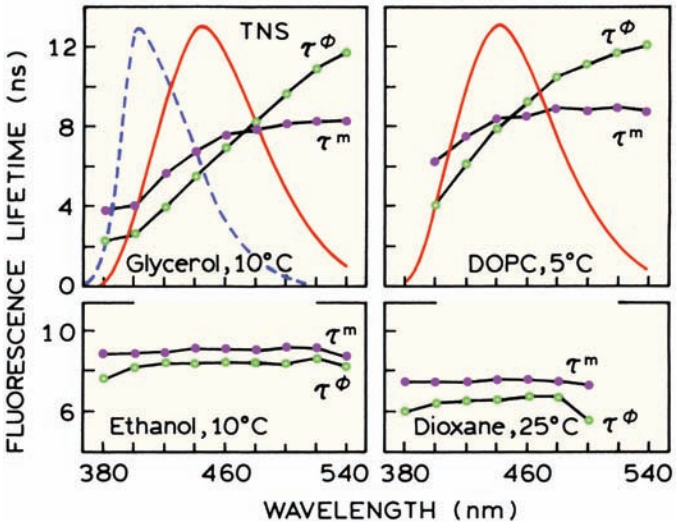

Figure 7.57. Fluorescence lifetimes and spectra of TNS, dissolved in various solvents and TNS bound to DOPC vesicles. Apparent phase shift (○) and modulation (●) lifetimes were measured at 30 MHz. Normalized emission spectra are shown for TNS in glycerol and bound in DOPC vesicles (solid), and for TNS in dioxane at 25°C (dashed).

P7.3. *Lifetime of the R State*: Use the data in Figure 7.53 to calculate the decay time of the 2-PI excimer emission, assuming this state could be excited directly.

P7.4. *Interpretation of Time-Resolved Decays of Acridine*: The excited-state protonation of acridine was examined by time-resolved measurements of the fluorescence decays.[139] Neutral acridine is protonated in the excited state by ammonium ions. The impulse response functions for acridine in 0.2 M NH_4NO_3, pH = 8.3 (Figure 7.49), are listed in Table 7.6.

A. If available, how would you use the absorption spectra of acridine in 0.05 M NaOH, 0.05 M H_2SO_4, and 0.2 M NH_4NO_3 to distinguish between ground-state and excited-state protonation of acridine?

B. What characteristics of the data in Table 7.6 most clearly illustrate that an excited-state reaction is present? Do these data indicate a two-state reaction or some more complex process? Is the reaction reversible or irreversible?

P7.5. *Interpretation of TRES*: Figure 7.58 shows time-resolved emission spectra of the solvent-sensitive probe 1-anilinonaphthalene (1-AN) in glycerol.[163] The TRES were obtained using excitation in the center of the absorption band (337 nm) and excitation on the red edge of the absorption (416 nm). Explain the difference between these TRES.

Table 7.6. Time-Resolved Decays of Acridine in 0.2 M NH_4 NO_3[139]

λ (nm)	α_1[a]	τ_1 (ns)	α_2	τ_2 (ns)
400	0.503	3.94	–0.001	33.96
410	0.220	4.00	–	–
420	0.491	3.88	0.002	25.20
450	0.067	3.90	0.028	30.05
500	–0.010	4.91	0.082	29.13
540	–0.036	3.76	.064	29.83
550	–0.036	3.56	.058	29.94
560	–0.029	3.86	.046	29.90

[a]The $|\alpha_i\tau_i|$ products are normalized to the steady-state emission intensity at each wavelength.

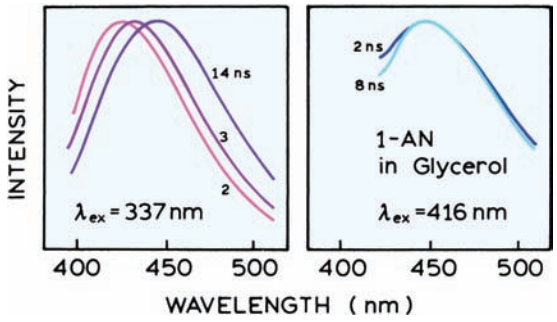

Figure 7.58. The time-resolved fluorescence spectra of 1-AN in glycerol at different excitation wavelengths. Left: 2 ns, 3 ns, and 14 ns after excitation. Right: 2 and 8 ns after excitation. Revised from [163].